



Performance of WRF Large-Eddy Simulations in summertime CBL characteristics over the Taklimakan Desert: A Real Test Case

Journal:	<i>Journal of Meteorological Research (JMR)</i>
Manuscript ID	ACTA-E-2018-0001.R1
Manuscript Type:	Original Article
Date Submitted by the Author:	19-Apr-2018
Complete List of Authors:	Xu, Hongxiong Wang, Minzhong Wang, Yinjun; Chinese Academy of Meteorological Sciences, State Key Laboratory of Severe Weather
Keywords:	WRF, Large Eddy Simulation, Convective Boundary Layer, Taklimakan
Speciality:	Large Eddy Simulation, Convective Boundary Layer

SCHOLARONE™
Manuscripts

1 **Performance of WRF Large-Eddy Simulations in summertime CBL**
2 **characteristics over the Taklimakan Desert: A Real Test Case**

3
4
5 Hongxiong Xu¹, Minzhong Wang^{1,2,4}, Yinjun Wang¹, Wenyue Cai¹³
6
7
8
9

10
11
12
13
14
15
16
17 1 State Key Laboratory of Severe Weather, Chinese Academy of Meteorological Sciences
18 Beijing, China 100081

19 2 Institute of Desert Meteorology, CMA (Chinese Meteorological Administration),
20 Urumqi, China

21 3 National Climate Center, Chinese Meteorological Administration,
22 Beijing, China 100081

23 4 Taklimakan Desert Atmospheric Environment Observation Experimental Station, Tazhong 841000,
24 China

25
26
27
28
29
30 Submitted to ***Journal of Meteorological Research***

31 January 2, 2018

32 Corresponding author:

33 Dr. Minzhong Wang

34 Institute of Desert Meteorology,

35 CMA (Chinese Meteorological Administration),

36 No. 46, Zhongguancun South Street, Haidian District, Beijing

37 P. R. China, 100081

38 Email: wangmz@idm.cn

39 dorn1984@163.com

40

41 **Abstract**

42 During the summer season over Taklimakan Desert, the maximum height of the CBL
43 (convective boundary layer) can exceed 5,000 m, which appeared to play critical roles in
44 simulating the regional circulation and weather. In this paper, we use a combination of WRF-LES
45 (Weather Research and Forecasting Model Large-Eddy Simulation), the GPS radiosonde and
46 eddy-covariance station to evaluate the performance of WRF-LES in the deep convective PBL
47 case over the central Taklimakan. Results show that the model reproduces reasonably well the
48 evolution of PBL processes. However, simulations are relative warmer and moister than those
49 observed due to the over-predicted surface fluxes and largescale advection. Tests are further
50 performed with multiple configurations and sensitive experiments. Sensitivity tests to Lateral
51 Boundary Condition(LBC) showed that the model results are very sensitive to changes in time
52 resolution and domain size of Specified LBC. It is found that larger domain size varies the
53 distance of the area of interest from the LBC, is efficient to reduce the influences of large forecast
54 error near the LBC. However, more frequently updated LBC is desirable to inhibit model error
55 near the LBC. On the other hand, model error increased as the distance between the area of
56 interest and the lateral boundaries decreased. Furthermore, comparing model results using the
57 original surface land parameterized sensible heat flux(SH) with Noah land-surface scheme and
58 those of sensitive experiment, it is concluded that the desert CBL is very sensitivity to SH
59 produced by surface land scheme during summer day time. A reduction in SH can correct
60 overestimate of the potential temperature profile. However, increasing SH significantly reduce the
61 total time needed for CBL increase to a relative low altitude (< 3 km) at the middle and
62 preliminary stage of the development of CBL rather than produce higher CBL at the late stage

63 Keyword: WRF, Large Eddy Simulation, Convective Boundary Layer, Taklimakan

64

65

For Review Only

66 1 Introduction

67 The Taklimakan Desert, locates at the south center of the province of Xinjiang, China, is
68 the world's second-largest flow desert and has profound influences on the regional weather
69 and climate. Because of the extreme near-surface temperatures, the Taklimakan PBL
70 (planetary boundary layer) commonly reaches 4–6 km during boreal summer(Wang et al.),
71 making it probably the deepest on earth. The deep PBL, which is significantly higher than that
72 of the surrounding mountains and oases, appeared to play important roles on regional
73 circulation and weather. In the northwest of china, the ability to accurately forecast in
74 Taklimakan Desert especially the PBL processes is an important problem.

75 The large desert (such as Sahara, Taklimakan et al.) atmosphere is always a key
76 component of the climate system. The surface heating from intense solar radiation leads to the
77 development of a near-surface thermal low pressure system, commonly referred to as the heat
78 low(Engelstaedter et al. 2015). However, despite of the vital role of the desert playing in the
79 climate system, observations are extremely sparse, and thin data that exist are mostly from the
80 surrounding of the desert due to the poor work and natural(Marsham et al. 2011). This
81 fundamentally restrict the development of understanding desert and surrounding area, and
82 leads to large discrepancies to analyses and significant biases in operational numerical
83 weather prediction (NWP) models, given the scarcity of observation being assimilated by
84 operational systems. The ability of these local models to simulate real-world cases is often
85 hindered by a lack of favorable data needed to assess the performance of model
86 results(Garcia-Carreras et al. 2015). To fill in the gaps of Taklimakan desert, the field
87 observation experiment was held during the month of July 2016 in Tazhong, which is located

88 at center of Taklimakan, by the Institute of Desert Meteorology (IDM), Chinese
89 Meteorological Administration (CMA), Urumqi(Liu et al. 2012; WANG et al. 2016a; Wang
90 et al. 2016b). This will also give the opportunity to evaluate the performance of the deep PBL
91 process in NWP models over Taklimakan.

92 On the other hand, atmospheric motions interweave small-scale, complex and multiscale
93 nonlinear interactions. Due to the limited resolution (time and space) mesoscale atmospheric
94 models are still unable to explicitly represent all these processes(Talbot et al. 2012). Such
95 processes include turbulent motions, which are too small-scale to be explicitly resolved in the
96 atmospheric model by a simplified process. Furthermore, turbulent mixing throughout the
97 PBL can heavily impacted NWP forecasting (Shin; Hong 2011; Shin; Hong 2015).

98 One way to tackle complex turbulent flows in weather forecast models is Large eddy
99 simulation (LES) which explicitly resolve energy-containing turbulent motions that are
100 responsible for most of the turbulent transport(Moeng et al. 2007). It has been used
101 intensively to examine detailed turbulence structure, to generate statistics, and to perform
102 physical-process studies(Garcia-Carreras et al. 2015; Heinold et al. 2013; Heinold et al. 2015;
103 Heinze et al. 2015; Sun; Xu 2009). However, most LES applications to the PBL have been
104 limited to idealized physical conditions. Recently, some studies attempt to test LES and assess
105 its performance in simulating real cases(Liu et al. 2011; Talbot et al. 2012). Liu et al. (2011)
106 suggests that WRF-LES is a valuable tool for simulating real world microscale weather flows
107 and for development of future real-time forecasting system, although further LES modeling
108 tests, such as elucidate whether inaccurate synoptic forcing or coarse resolution, are highly
109 recommended. Talbot et al. (2012) suggested that the ability of WRF-LES to simulate

110 real-world cases are hindered by a lack of favorable synoptic forcing. The initial(ICS) and
111 lateral boundary conditions(LBCS) was found to be more critical to the LES results than
112 subgrid-scale turbulence closures. Thus, the LBCS of can significantly alter high-resolution
113 LES status through inflow boundaries(Rai et al. 2017).

114 However, most of research above on LES over desert has been limited to idealized
115 physical conditions(Garcia-Carreras et al. 2015) or conducted real case outside
116 Taklimakan(Liu et al. 2011; Talbot et al. 2012). The aim of this study is the attempt to
117 applicate LES in a real deep CBL case over Taklimakan. An important aspect of the ongoing
118 this paper is to examine assess the skillfulness of WRF-LES in relative coarse resolution
119 (333m) over Taklimakan dessert in simulating real cases of deep desert PBL process during
120 boreal summer events in Taklimakan. First we use a combination of WRF-LES and the GPS
121 radiosonde and surface fluxes calculated by an eddy-covariance method taken in the central
122 Taklimakan to evaluate the performance of WRF-LES in real case. Then we assess the
123 potential errors related to LBC. Moreover, we aim to evaluate the relative contribution of
124 uncertainties in surface model to the typical behavior of PBL processes by conducting the
125 sensitivity experiments. Thus, the sensitivity of the performance to surface sensible heat flux
126 (SH) is also studied. Section 2 gives a brief description of synoptic of the study case, and we
127 described data and model configuration and design of numerical experiments used in this
128 study. We presented the results of numerical simulations in Section 4. Finally, we summarize
129 conclusions in Section 5.

130 2 Method

131 2.1 Model configuration

132 The WRF model of version 3.8.1 (Skamarock et al. 2008) is utilized here at
133 sub-kilometer resolutions to simulate the extreme CBL event in Taklimakan desert. The
134 model is integrated for 12h, starting from 0800 BJT (Beijing Time) 01 Jul 2016. We
135 conducted one-way nest WRF from mesoscale down to LES-scales. All domains were 51
136 levels extended to 50 hPa. Height for lowest 20 levels are 1130.473, 1157.705, 1207.765,
137 1294.703, 1423.873, 1591.895, 1795.526, 2021.868, 2272.33, 2558.433, 2882.675, 3248.113,
138 3658.499, 4118.481, 4633.882, 5212.111, 5855.802, 6517.111, 7151.295, 7757.151. The
139 model horizontal spacing is 12km 3km 1km and 0.33km for d01 d02 d03 and d04. The sizes
140 of model grids are 411 ×321 791x651 211x201 and 403x406 respectively. Figure 1 shows
141 the domain for all experiments except for BDY_T3. Smaller grid sizes (205 X 208) are used
142 in experiment BDY_T3 to verify the effect of domain size on LES simulation.

143 The initialized condition and lateral boundary conditions are provided to the coarsest
144 mesoscale simulations from NCEP Global Data Assimilation System (GDAS) Final
145 Operational Global Analyses. The analyses are 0.25-degree by 0.25-degree grids prepared
146 operationally every six hours and available on the surface, at 32 mandatory (and other
147 pressure) levels from 1000 millibars to 10 millibars (National Centers for Environmental
148 Prediction 2015).

149 The model physical options include the WSM5 microphysics scheme (Hong; Lim 2006),
150 the Yonsei University (YSU) planetary boundary layer scheme (Hong; Pan 1996), the Kain–
151 Fritsch cumulus parameterization scheme(Kain 1993; Kain 2004), RUC (Rapid Update Cycle)
152 land-surface model(Smirnova Tatiana et al. 2000; Smirnova et al. 1997), the Rapid Radiative
153 Transfer Model (Mlawer et al. 1997) longwave, and the Dudhia shortwave radiation scheme

154 (Dudhia 1989). The cumulus parameterization scheme is only applied to the d01(12km) grid
155 domain to parameterize the convective rainfall. While, the large-eddy-simulation (LES) is
156 only applied to d04(0.333km).

157 Table 1 shows the list of experiments. Experiment 1 was the control experiment, denoted
158 as CTRL. The experiment 2 (6-hour update LBC, denoted BDY_T2) and experiments 3(with
159 domain sizes 205 X 208, denoted BDY_T2) were conducted the same as CTRL with different
160 domain sizes and LBC update frequency. In experiment 4 (denoted HFX_%75) and 5
161 (denoted HFX_%125), the SH (sensible heat flux) was reduced to 75% and 125% of that in
162 the control experiment in the RUC land-surface scheme, to highlight the impact of SH on
163 deep CBL at Taklimakan desert, respectively. In experiment 6 (denoted Noah), Noah
164 land-surface model(Chen; Dudhia 2001a, 2001b) was used to replace the RUC land-surface
165 model in CTRL experiment to discriminate the influence of different land-surface model on
166 deep CBL.

167 2.2 Data

168 The model simulations are compared to the Tazhong field experiment, which was held
169 during the whole month of July 2016 in Tazhong, by the Institute of Desert Meteorology
170 (IDM), Chinese Meteorological Administration (CMA), Urumqi. The main station was
171 located at 86.63° E, 39.03° N. The location is relatively flat with few hills and covered by
172 sand combined with grass (Figure 1), and the deep PBL of our simulation was under a
173 cloudless sky and dry environment. Instruments are described as follows:

174 1) surface fluxes: The eddy correlation system was a R3-50 supersonic anemometer
175 developed by Gill Company, UK, deployed at a height of 10 m. The data acquisition

176 frequency was 20 Hz, and the surface sensible heat flux was calculated by the
177 eddy-covariance method.

178 2) vertical profiles measured using soundings: Upper air soundings of temperature,
179 pressure, humidity, and wind speed and direction were conducted 3-6 times per day with the
180 GPS sounding system developed by No. 23 Institute of China Aerospace Science & Industry
181 Corp. (CASIC23). The sounding times were 01:15, 07:15, 10:15, 13:15, 16:15 and 19:15
182 respectively.

183 2.3 Synoptic

184 Figure 2 shows the synoptic patterns at 0800 BJT 1 July 2016 at 850 700 500 and 100
185 hPa. There were cyclonic vortex from 850 to 500 hPa center at 55° N (Figure 2a ,b and c).
186 Taklimakan was located east of cyclonic vortex and embedded in east–west-elongated ridge
187 at 0800 BJT 1 July. To the southwest, influenced by the South Asia High, which was centered
188 over the eastern Iranian Plateau, the upper air over the Taklimakan Desert was controlled by
189 the westerly jet stream at 100hPa (Figure 2 d). The low-pressure system at low level, which
190 is termed of heat low (Figure 3), dominated most area of southern Xinjiang and resulted in
191 continuous high temperature over the desert. This situation favored the subsidence motion and
192 served as a triggering mechanism for deep PBL in the region in the coming 2–3 days (not
193 show).

194 3 Results

195 3.1 Validation of the deep CBL structure

196 Time series of surface variables at Tazhong station from CTRL simulation for 01 July
197 2016 are presented in Figure 4a, b. Results show that discrepancies of thermodynamic surface

198 variables (the surface temperature, sensible and latent fluxes) between model and observation
199 are large during simulation. The SH (surface sensible heat flux) is far less in observation
200 (maximum: 243 W m^{-2}) relative to model (maximum: 613 W m^{-2}). This represents SH from
201 WRF simulation is 2.5 times than that of observation when both of which reach its maximum.
202 On the other hand, model shows a significant cold bias for the surface temperature. The
203 surface temperature is much higher in observation (maximum: $70 \text{ }^\circ\text{C}$) relative to model
204 (maximum: $50 \text{ }^\circ\text{C}$). To further verification the surface variables, RMSE (root mean squared
205 error) and BIAS (mean bias) are calculated including integration hours from 3 to 12 h for
206 Tazhong station in Table 2. As mentioned earlier, model show yields significantly
207 overestimate of SH (RMSE 263.636 W/m^2 , BIAS: 250.14 W/m^2) and dramatically
208 underestimated of surface temperature (RMSE $14.65 \text{ }^\circ\text{C}$, BIAS: $-13.37 \text{ }^\circ\text{C}$).

209 Two possible reasons result in model SH far above that of observation: (1) The
210 mismatches of land-use between the model and the observation. WRF use land-use categories
211 to assign certain static parameters and initial values to each grid cell, for example, albedo,
212 surface roughness, and so on (Schicker et al. 2016). However, As in Figure 1c, the EC station
213 is surround by mixing land of grass and sand. The complex underlying surface may not be
214 adequately reproduced by model and can have an impact on the overestimate of SH in this
215 case. (2) It is should be noted that the SH and LH (latent heat flux) based on eddy
216 correlation might be underestimated (LeMone et al. 2013). Researchers found that if the other
217 two terms in the budget—net radiation and flux into the soil were accurate, used data for the
218 whole experiment to find the $H + LE$ for Tazhong station are equal to an average of 75% of
219 what would be required for balancing the surface energy budget.

220 Despite the large differences on surface, near-surface variables (2m temperature, relative
221 humidity and 10m wind speed, Figure 4 e f g) are closer to measurements than those from
222 surface, their values are relatively higher than those observed. The time series evolution of 2m
223 temperatures nearly follow those of the observations (RMSE:1.66, BIAS:1.61); but model
224 produce warmer surfaces by about 3 K at the beginning of model integration, and 1K when
225 model and observation both reach their maximum temperature, respectively.

226 Results indicate that, model-produced near-surface relative humidity is close to
227 observations at initial time (Figure 4 f). However, the humidity from the model keeps
228 increasing at the first few hours of model integration, when observations decrease. After 3
229 hours' spin-up, the model reproduces reasonably well the evolution of humidity, in agreement
230 with observation (RMSE:1.22), but their values are relative higher than those
231 observed(BIAS:1.11).

232 One reason for this discrepancy is the overestimate of soil moisture during simulation.
233 Soil moisture can severely impact near-surface humidity. The overestimate of the soil
234 moisture contents in the initial condition of the model, which are only offered to the model at
235 initial time, may result in considerable differences in near-surface layer humidity (Talbot et al.
236 2012). In the present simulations, model results are reported to produce grossly overestimate
237 soil moisture. At the model initialization for the CTRL simulation, EC station at Tazhong
238 station indicated a value of the 5-cm-deep soil moisture of $0.230 \text{ m}^3/\text{m}^3$, while the model
239 initial value is $0.6 \text{ m}^3/\text{m}^3$ (Figure 4 d). This large overestimate of soil moisture results in LH
240 (Figure 4 b, f) from the model continue to increase. As a result, near-surface of model is far
241 moister than that of observation at the first few hours of model integration. An interesting

242 result to note is that the model simulation has the abilities to correct some of the bias due to
243 the initial condition of the surface; The results from CTRL experiment are closer to
244 observation after 3 hours' spin-up.

245 The model simulated potential temperature are compared to GPS sounding
246 measurements at Tazhong during 0800~2000 BJT 01JULY2016 in Figure 5 (solid lines). One
247 should note that radio-sounder floating about 7 Km away from Tazhong, when radio-sounder
248 reach 6 Km height. Thus, for comparison, the profiles of model simulations are averaged
249 station in a radius of 3.5 Km. At 0800 BJT, when the model is initialized, the nocturnal
250 inversion reaches 300m (not shown). By 1100 BJT, this inversion is eroded in the model in
251 agreement with observations, and both reaching about 300m at 1100 BJT (Figure 5 a).
252 However, the simulated CBL grows faster in the morning due to larger SH than observation,
253 reaching 3500m (3000m in the observations) at 1400 BJT (Figure 5 b). At 1700 BJT (Figure 5
254 c), the simulated and observed CBL heights exceed 4000m and 5000m respectively. This
255 indicates that the simulated CBL grows more slowly in the afternoon than measurement.
256 Compared to measurements, the model is initially cooler with faster heating rate in the
257 morning. As a result, model is warmer than measurements in the afternoon. Eventually, model
258 agrees with observations at the end of the day. One possible minor reason is the differences of
259 potential temperature lapse rate above the top of mixing layer between observation and
260 simulation. Simulated stronger inversion layer restrain the development of CBL, which will
261 be discussed below.

262 Moreover, in terms of CBL temperatures, the model initially simulates a cooler and drier
263 CBL than that observed, at 1100 BJT01 JUL (Figure 5a). Compared to the observed potential

264 temperature profile, the CBL seems to appear earlier in model forecasts result based on
265 obvious warming in surface layer. One should note that RL (residual layer) may play a key
266 role in the deep PBL at Taklimakan desert. At 1100 BJT, when the CBLH was about 300 m in
267 observation as show above, potential temperature in the were about 317 in PBL and 320 K in
268 RL, respectively. When the potential temperature in CBL increased to the value in RL (320
269 K), the CBL merged with the RL, and the height of PBL reach 3000m in the observations at
270 1400 BJT. These results are in good agreement with Han et al. (2012). By analysis of
271 observation of a CBL in the Badanjilin region, they found a rapid development process of
272 CBL after 1200 LST, which appeared to be a jump of CBLH when the inversion layer
273 vanished.

274 When the SH reaches its maximum at 1400 BJT (Figure 5b), potential temperature
275 profile is closer to measurements than at initial time, and their values are higher than those
276 observed. By 2000 BJT (Figure 5d), CBLH in the model reaches its maximum value, which is
277 consistent with observation, despite of approximately 0.4K cooler on the lower
278 levels(<2.5Km). As mentioned, one cause of the higher temperatures produced with
279 model would be the large difference in the surface heat fluxes. It was concluded that
280 the surface sensible heat flux from the land surface parameterization is the crucial
281 factor affecting the CBL process during summer day time. Differences in surface SH
282 would create differences in the vertical development of the PBL. Thus, the large
283 surface SH difference between the model and observation may lead to differences in
284 CBL growth during daytime and in its peak depth during the simulation. Fortunately,
285 one can artificially modify the surface SH computed by surface-land model, which

286 controls the calculation of surface fluxes. Sensitive simulations will be realized and
287 discussed in next section.

288 Figure 5 also shows Vertical profiles of vapor mixing ratio (dash lines) at Tazhong
289 station. The simulated profiles with lower RL are much drier than observation from 1500 to
290 3500m at 1100 BJT. The vertical mixing results in the uniform structure of vapor mixing ratio
291 within CBL, so the differences between simulated and observational profiles are reduced
292 remarkably when CBL reach above 4000m at 1400 BJT. Differences are generally less than
293 1g/Kg at 1100 BJT reaching a maximum of 0.3g/Kg at 1400 BJT. However, measured PBL
294 moisture shows an inverse layer at lower PBL(≤ 2000 m) range from 2.8 to 3.6 g/Kg, which is
295 not captured by model. Furthermore, as the convective boundary layer grows, the inversion
296 moisture structure below 3000m develops to and maintains below 3000m during 1400~2000
297 BJT. By the end of the day, the model-simulated CBL humidity show moister than
298 observation, because model cannot reproduce the inverse moisture layer within CBL.

299 Inverse humidity may be caused by the joint of the heterogeneous humidity Pattern and
300 Large-scale advection over the underlying surface. For instance, interaction of oasis with
301 desert environment may resulted in the inverse humidity layer in desert PBL. Thus, one
302 possible reason for the discrepancy between model and observation caused by the error in
303 land-use type. The USGS land-use in ARW-WRF is based on AVHRR (Advanced Very High
304 Resolution Radiometer) 1km resolution satellite data during 1992-1993. For our case, this
305 land-use data may be outdated in Taklimakan. Besides such changes, misclassifications are
306 found in the USGS land-use data, the default land-use dataset in WRF(Schicker et al. 2016).
307 This is also confirmed by the discrepancies of land-use between simulation and measured at

308 the Tazhong station in the previous figure. Large-scale advection of dry air can affect the
309 profile of moisture. Moisture will also be variable in the horizontal, so advection at the low
310 level could contribute to the dry at bottom and moisture at the upper of PBL between 1100
311 and 2000 BJT at the bottom of the PBL.

312 The mismatch between the model and the observations in terms of moisture that is
313 present means that the effect of land-use type and Large-scale advection needs to be
314 quantified and that more detailed data of Taklimakan (land and atmosphere) might be
315 necessary to realize a more realistic performance. Extra care should also be taken with sparse
316 and the limited data in the periphery of the Taklimakan (ter Maat et al. 2012).

317 **3.2 Sensitive to Lateral Boundary Condition(LBC)**

318 After verifying the details of the LES simulations, we assess the sensitivity of the LES
319 simulations to time resolution and domain size of Specified LBC. For one-way nest, Specified
320 LBC is obtained from coarser model simulation. The analysis and all forecast times from a
321 previously-run larger-area model simulation are used to specify the LBC. The primary cause
322 of differences in PBL structure was diagnosed as differences in domain size and frequency
323 provided by the coarser resolution. The aim is to assess the sensitivity of the finer large-eddy
324 simulations to time frequency and domain size of Specified LBC forcing by larger-area model
325 simulation; Details of the three simulations (CTRL, BDY_T2 and BDY_T3) are given in
326 section 2.

327 Figure 5 compare the profiles of the simulated potential temperature and vapor mixing
328 ratio profiles from LBC sensitivity experiments and observation. Results indicate that, there is
329 a distinct relationship between LBC and CBL development. All model-produced profiles are

330 nearly the same at initial time (not show). However, the comparison results reveal that
331 discrepancies among different experiments are large for CBL. The results indicate that larger
332 domain size and more time frequency LBC leads to a warmer and drier PBL, but a cooler and
333 moister free troposphere. Such sensitivity is monotonic with respect to LBC (Figure 5).
334 Furthermore, in the next three hours, the differences between the sensitive experiments keep
335 increasing with time (Figure 5 a, b). The potential temperature profiles within CBL become
336 divergence at 1100 BJT. However, the results show more convergence at afternoon as CBL
337 continues to grow (Figure 5 c). Finally, largest discrepancies are found by end of the day
338 (Figure 5 d) where the model CBL potential temperature is warmer by up to about 0.7K and
339 0.9K in BDY_T2 and BDY_T1 respectively, compared to measurements.

340 Figure 6 shows cross sections along 39.03°N of horizontal winds, superposed with theta
341 and vapor mixing ratio. Overall, the lower frequently updated LBC is desirable to cold zone
342 near the LBC, which results in cold advection of the temperature and moisture to the area of
343 interest (Figure 6 b, c). Larger domain size, which varies the distance of the area of interest
344 from the LBC, is efficient to reduce the influences of large forecast error near the LBC to the
345 area of interest (CMP Figure 6 a, c). The results suggest that the model results are sensitive
346 to changes in time resolution and domain size of Specified LBC. The mismatch among
347 sensitive experiments is present means that the effect of LBC needs to be quantified to realize
348 a more realistic performance in the sub-kilometer simulations.

349 To further examine the impact of LBCS on the turbulence of deep Taklimakan desert
350 CBL, the instantaneous vertical velocity fields for the horizontal are displayed in . By 1400
351 BJT, the convection of CTRL simulation obviously intensified under strong surface heating

352 (Xu et al. 2018). Thus, the maximum vertical velocity reaches 9 m/s and the depth of mixed
353 layer grows to about 4.3 km (a). The distances between the boundary layer rolls
354 correspondingly increase to about 12 km and the height of the peak updraughts is raised to
355 just under 4 km. The cellular shape of updraughts and downdraughts characteristic of
356 boundary layer rolls is obvious in the horizontal view with the strength of convection.
357 BDY_T2 and BDY_T3 experiments (b, c) both reproduce motions with much weaker
358 maximum and minimum values at boundary of domain. In BDY_T3 experiment, Tazhong
359 station at center of the model has been directly influenced by the inflow cold advection
360 produced by low frequency LBCS and results in much weaker maximum and minimum value
361 of w (about 6 m/s). However, despite the underestimate of potential temperature, the w fields
362 for BDY_T2 experiment look similar to the CTRL w in plain view, and the horizontal extent
363 of the updrafts/downdrafts agrees with the CTRL as can be inferred from . To further examine
364 vertical structure of desert CBL, vertical cross-sections along Tazhong station (39°N) of w
365 are presented in Figure 8. Wide and regularly spaced updrafts along A1- A2 split into the
366 stronger and more irregular motions in CTRL and BDY_T2. The updrafts are much weaker in
367 the BDY_T3 experiment, as can be seen from Figure 8 c. Peak updrafts on BDY_T3 are about
368 4 m/s much weaker than on CTRL (9 m/s) and BDY_T2 (8 m/s). For BDY_T2 and BDY_T3,
369 the distant of the inflow boundary is wider, and the intensity of the convection is weaker at
370 the boundary. Compared with BDY_T2, the horizontal distribution of vertical velocity at
371 Tazhong station in BDY_T3 experiments is much weaker.

372 **3.3 Simulations with different surface sensible heat flux (SH) and surface-land** 373 **models**

374 The import cause of differences in PBL structure was diagnosed above as differences in
375 SH predicted by the surface-land schemes. The SH is one of the key factor affecting the
376 CBLH during summer day time. Thus, the difference between model and observation may
377 lead to differences in PBL growth during daytime; To further confirm whether this indeed
378 occurs, three additional sensitive simulations were realized based on the CTRL experiment.
379 For Noah experiment Noah land-surface model is used to replace RUC land-surface model in
380 CTRL experiment, and for HFX-125%, HFX -75% SH is %125 and %75 that of CTRL (HFX
381 -100%) experiment, while the other parameters remain the same.

382 The results from Figure 10 and Table 2 showed that HFX-75% successively improved
383 the simulation of SH with RMSE:151.12, compared that of 263.64, 357.11 in CTRL and
384 HFX-125%. Of interesting is that experiment with Noah surface-land yielded the best
385 performance among all of the cases in SH, surface temperature and air temperature. However,
386 Noah surface-land model show large discrepancies with observation in Soil moisture, and
387 results in dramatically overestimate of LH and relative humidity compared to CTRL.

388 Further examining potential temperature and vapor mixing ratio (Figure 9) indicate that
389 with smaller SH leads to a cooler, moister lower PBL and a warmer, drier free atmosphere.
390 Such sensitivity is monotonic with respect to SH. Overall, the CBL structure from the
391 HFX-75% and Noah experiments match the GPS measurements better than the CTRL
392 (HFX-100%) simulations. Potential temperature profiles from CTRL (HFX-100%) and
393 HFX-125% are consistently warmer than the observation by about 0.4 and 0.5 K respectively,
394 while results from HFX-75% and Noah are within about 0.2K at 1400 BJT (Figure 9 b). The
395 results suggest that the model results are sensitive to changes SH from land-surface model.

396 However, simulations converge at the end of the day, but remain differences at 2000 BJT
397 (Figure 9 d). HFX-75% and Noah with weaker surface sensible heat flux can still produce the
398 deep CBL nearly the same as CTRL and HFX-125%. This indicates that SH may not be the
399 dominant factor for the deep CBL over the Taklimakan desert.

400 Results of simulations on desert PBL in the morning agree with the previous studies of
401 sensitivities land-surface model for other areas (Hu et al. 2010; Zhang et al. 2017). However,
402 during 1700~2000 BJT 01July (Figure 9b, d), all experiments produce nearly the same CBLH
403 and moisture in agreement with observation in the PBL. The effects of SH on the evolution of
404 Taklimakan PBL structures during this period are needed to be further examined and
405 discussed. So, the question is: why are simulations insensitive to land-surface process by the
406 end of the day? As in Stull (1988), the development of CBL is mainly influenced by the effect
407 of thermodynamic and turbulent entrainment without considering large scale factors such as
408 large scale advection or subsidence. Besides the surface sensible heat, the intensity of
409 entrainment process determines the increasing rate of CBL. Thus, the entrainment rate w_e is a
410 valuable indicator for the development of PBL structure.

411 The rate of growth of the convective boundary layer is mainly determined by the
412 entrainment rate w_e at the inversion layer without considering large scale vertical motion. w_e
413 usually has a positive correlation with heat flux amount at the inversion layer $\overline{(w'\theta_v)'}_h$, and
414 large LES experiments show $\overline{(w'\theta_v)'}_h$ is about 0.2 times the surface flux of buoyancy
415 $\overline{(w'\theta_0)'}$. During the period from 1100 to 1400 BJT, larger SH is obviously correlated with
416 stronger turbulent entrainment and warmer air from free atmosphere (FA) entraining into ML.
417 As a result, CBL develop rapidly and is warm too fast in the early simulation phase due to the

418 obviously increasing temperature and strong vertical mixing in model. Of interesting is that
419 reduction in SH reproduces better desert PBL evolution in the early simulation phase, as
420 SH-75% and Noah produce the smallest simulation errors in both temperature and moisture.
421 However, one should note that CBLH and potential temperature for SH-75% and Noah have
422 reached above 5000 m and 323.2 K respectively at 1700 BJT (Figure 9 a). For the rest of the
423 day, the increase rate of CBL height slows down due to the deep CBL(>5000m) which require
424 more heat for the growth of PBL depth; Moreover, w_e decrease with increasing inversion
425 intensity, which inhibits the mixing and entrainment processes. These two factors obviously
426 limit the growth of CBL when CBLH is over 5000 m in this deep desert CBL case. Therefore,
427 increasing SH from 75% to 125% significantly reduce the total time needed for CBL increase
428 to a relative low altitude (< 5 km) at the middle and preliminary stage of the development of
429 CBL rather than produce higher CBL at the late stage. When height of CBL over Taklimakan
430 desert exceeds 5000 m, it might not change with proportion to SH fluxes (Figure 9 d). As a
431 result, PBL of WRF simulations are basically the same, and not sensitive to SH fluxes by the
432 end of the day.

433 **4 Summary**

434 This paper assesses the performance of the Weather Research and Forecasting Model
435 (WRF) Large-Eddy Simulations(LES) in deep convective PBL case over Taklimakan Desert.
436 Tests are performed with multiple configurations and sensitive experiments. Sensitivity tests
437 to Lateral Boundary Condition(LBC) showed that the model results are sensitive to changes
438 in time resolution and domain size of Specified LBC. It is found that larger domain size varies
439 the distance of the area of interest from the LBC, is efficient to reduce the influences of large

440 forecast error near the LBC.

441 Consequently, with the configuration used in this study, the model reproduces
442 reasonably well the evolution of PBL processes. The model shows discrepancies between the
443 main CBL characteristics in the morning including the thermal and moisture structure. The
444 model simulates the relatively colder and drier morning CBL well, underestimating it by up to
445 1.5K near-surface layer at Tazhong station. In the case of the underestimation of moisture by
446 only up to 1 g/kg in the near-surface layer. The overestimation of CBL profile may be caused
447 by discrepancy between model and measurement initially. This indicates that the results are
448 sensitive to the model initial conditions. An interesting result to note is that the model
449 simulation seems to be able to correct some of the bias due to the initial condition. In the
450 afternoon, the model correctly reproduce the thermal structure, but simulations are relative
451 warmer and moister than those observed. Potential temperature profile at CBL appears
452 warmer by up to about 0.4K compared to the observations. While the model overestimates the
453 afternoon moisture seriously, it mainly overestimates vapor mixing ratio by about 1 to 2 g/Kg
454 in the CBL. Largest discrepancies are found in 0~3Km where the model vapor is twice as
455 moist (up to about 3g/Kg above AGL) as observed.

456 Furthermore, three additional sensitive simulations were realized to further confirm
457 whether large differences of SH lead to differences in ABL growth during daytime, based on
458 the CTRL experiment. The results suggest that the model results are sensitive to changes
459 SH and different land-surface models. The large difference between the model and
460 observation may lead to differences in CBL growth during daytime. From these results, it was
461 concluded the surface sensible heat flux is an important factor affecting the CBL depth over

462 Taklimakan during summer day time. However, its peak depth during the simulation show
463 less sensitive to SH because of decreasing w_e by the end of the day.

464 The future work aimed to study several other deep CBL cases over Taklimakan to
465 summarize their common features. Furthermore, we hope to utilize high resolution model and
466 observation to describe the fine characteristics of a typical deep Taklimakan CBL particularly
467 the turbulent and vertical mixing and its impact on regional weather forecast. This research is
468 aimed to improve the understanding of deep CBL over Taklimakan and its influence on
469 regional weather and climate.

470 **Conflict of Interests**

471 The author declares that there is no conflict of interests regarding the publication of this paper.

472 **Acknowledgments**

473 This study is supported by the National Natural Science Foundation of China (Grant no.
474 41575008 and 41775030). The author would like to thank all the reviewers and editors for
475 their professional advice to improve the paper.

476

477 Captions:

478 Figure 1 Simulation domains used in ARW model with terrain height (shaded, units:m); (b) land
479 use categories for domain D03 and D04.

480 Figure 2 Horizontal distribution of geopotential height (solid, units: dagpm), wind speed (shaded,
481 units: knot), and wind barbs from the NCEP FNL analysis at 0800 BJT 1 Jul 2016 at (a)
482 850 hPa, (c) 700 hPa, (e) 500 hPa, and (d) 100hPa.

483 Figure 3 NCEP FNL 700hPa potential temperature (colors) and mean sea level pressure (white
484 lines) at 0800 BJT 1 Jul 2016. The black dot shows the location of Tazhong station at
485 Xingjiang province.

486 Figure 4 Time series of simulated surface variables from innermost domain of simulations
487 and surface observations at Tazhong station (83.63° E, 39.03° N) initial at 0800
488 BJT 01July 2016 (a) sensible heat flux (W/m^2), (b) latent heat flux(W/m^2), (c) 2-m
489 temperature ($^{\circ}C$), (d) surface temperature ($^{\circ}C$), (e) 2-m Relative Humidity(%) and (f)
490 10-m wind speed (m/s) with corresponding observations.

491 Figure 5 Vertical profiles of potential temperature (solid line, units: K) and vapor mixing
492 ratio(dash line, units: g/Kg)from innermost domain of simulations and observation of
493 GPS sounding at Tazhong station (83.63° E, 39.03° N) at (a)1100 (b) 1400 (c)
494 1700 (d) 2000 BJT 01 Jul2016.

495 Figure 6 cross sections along $39.03^{\circ}N$ of horizontal winds (barbs, units: m/s), at intervals of 5 m/s,
496 superposed with theta (shaded, units: K) and vapor mixing ratio(contour, units: g/Kg), from (a)
497 BDY_T1, (c) BDY_T2, (e) BDY_T3 experiments at1400 BJT 01JUL2016, (b), (d), (f) are the
498 same as (a), (c), (e), but for 2000 BJT 01JUL2016.

499 Figure 7 Instantaneous vertical velocity fields (shading: m/s) at 3000 m for (a) BDY_T1 (CTRL), (b)
500 BDY_T2, (c) BDY_T3, and (d) Noah at 1400 BJT, 1 July 2016.

501 Figure 8 Vertical cross-section of instantaneous vertical velocity fields (shading: m/s) along
502 A1-A2 in for for (a) BDY_T1 (CTRL), (b) BDY_T2, (c) BDY_T3, and (d) Noah at 1400 BJT,
503 1 July 2016.

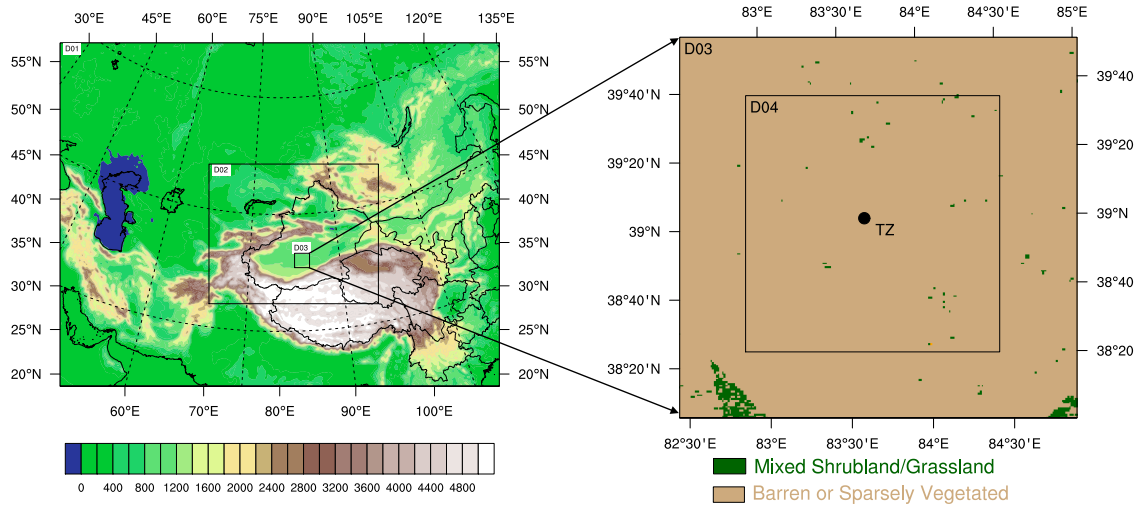
504 Figure 9 The same as Figure 5, but for SH flux sensitive and Noah land-surface experiment.

505 Figure 10 The same as Figure 4, but for SH flux sensitive and Noah land-surface experiment.

506

507

For Review Only



508

509

(a)

(b)



(c)

510

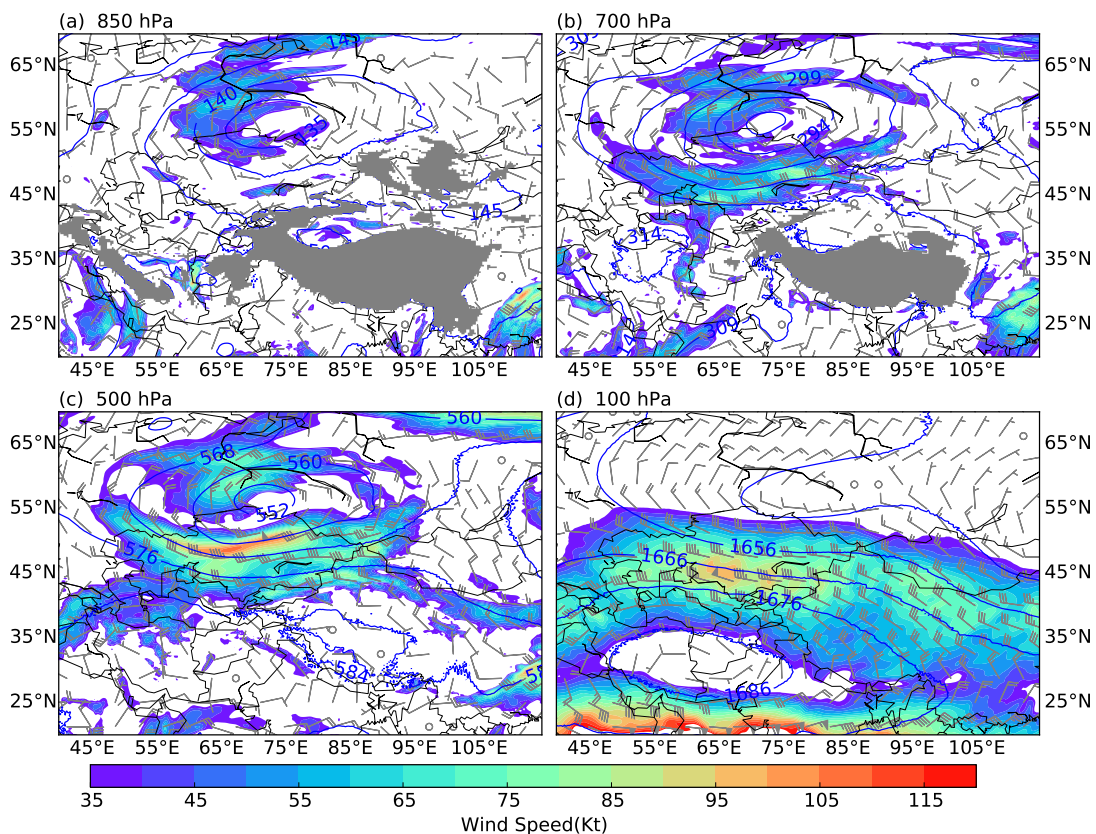
511

512 Figure 1 Simulation domains used in ARW model with terrain height (shaded, units:m); (b)

513 land use categories for domain D03 and D04; (c) photograph of Tazhong station

514

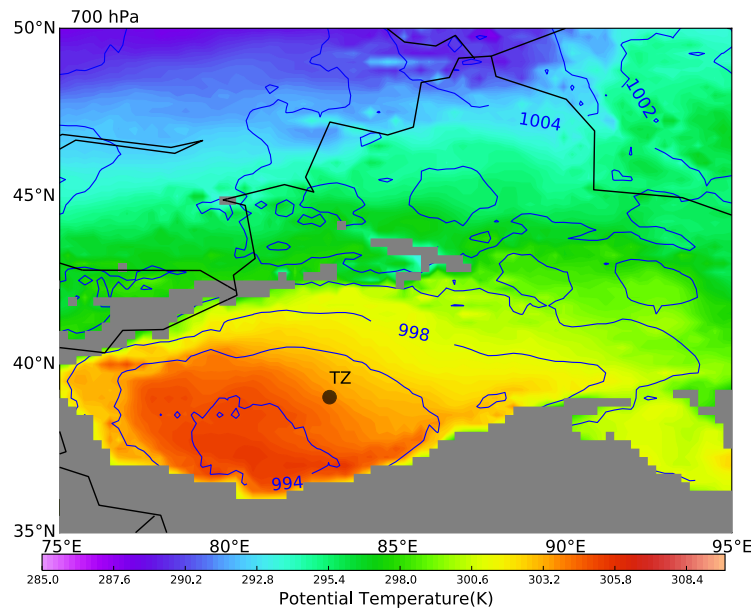
515



516

517 Figure 2 Horizontal distribution of geopotential height (solid, units: dagpm), wind speed
 518 (shaded, units: knot), and wind barbs from the NCEP FNL analysis at 0800 BJT 1 Jul 2016 at
 519 (a) 850 hPa, (c) 700 hPa, (e) 500 hPa, and (d) 100hPa.

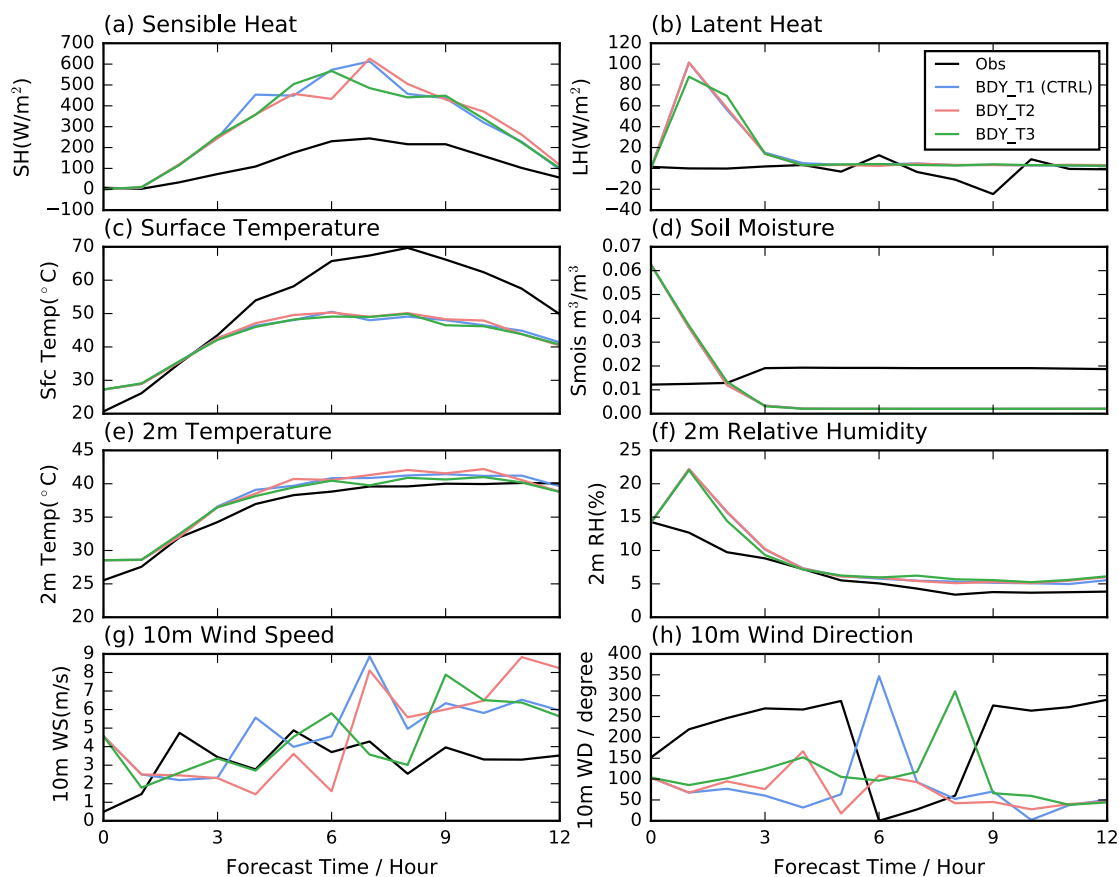
520



521

522 Figure 3 NCEP FNL 700hPa potential temperature (colors) and mean sea level pressure (white lines) at

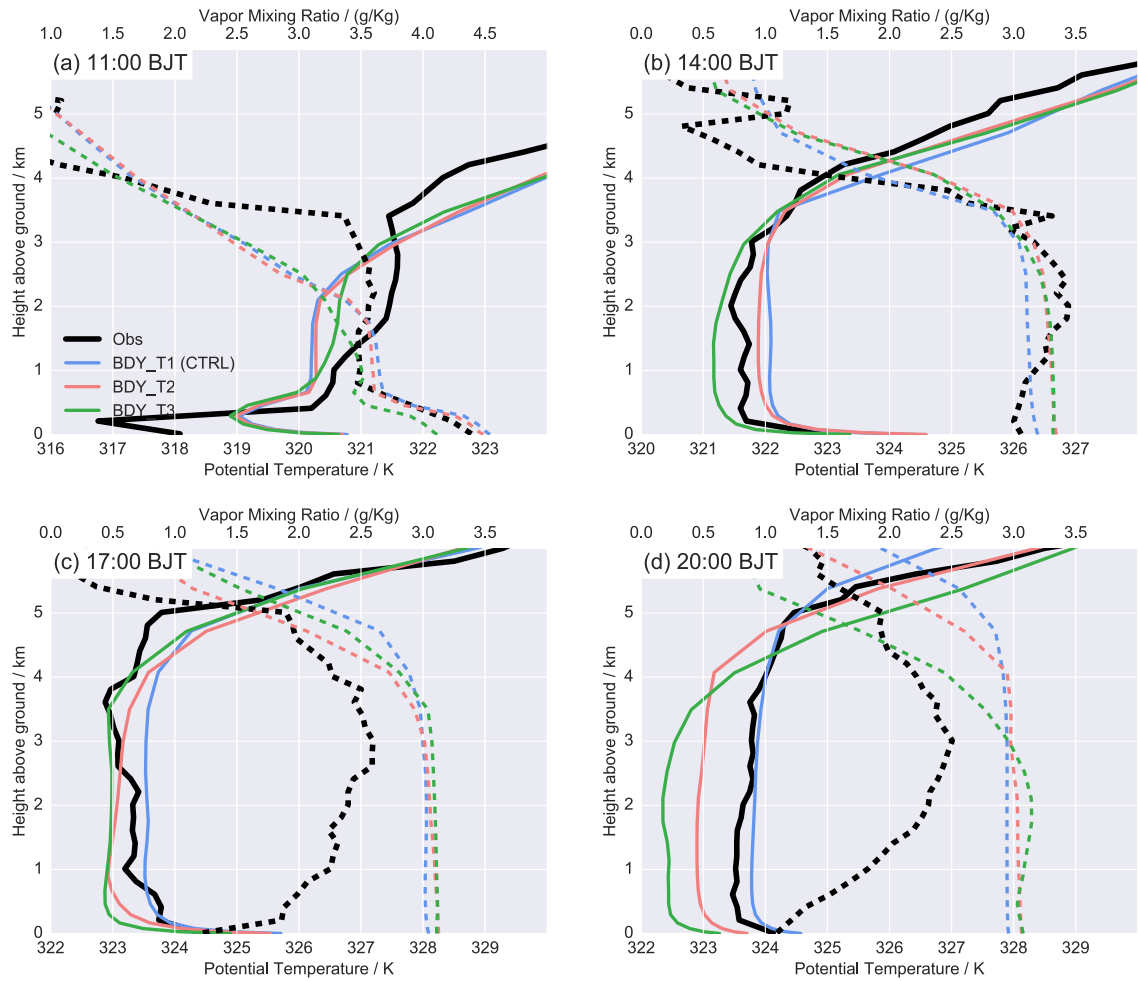
523 0800 BJT 1 Jul 2016. The black dot shows the location of Tazhong station at Xingjiang province.



524

525 Figure 4 Time series of simulated surface variables from innermost domain of simulations
 526 and surface observations at Tazhong station (83.63° E, 39.03° N) initial at 0800 BJT 01July
 527 2016 (a) sensible heat flux (W/m^2), (b) latent heat flux (W/m^2), (c) 2-m temperature ($^{\circ}\text{C}$), (d)
 528 surface temperature ($^{\circ}\text{C}$), (e) 2-m Relative Humidity (%) and (f) 10-m wind speed (m/s) with
 529 corresponding observations.

530



531

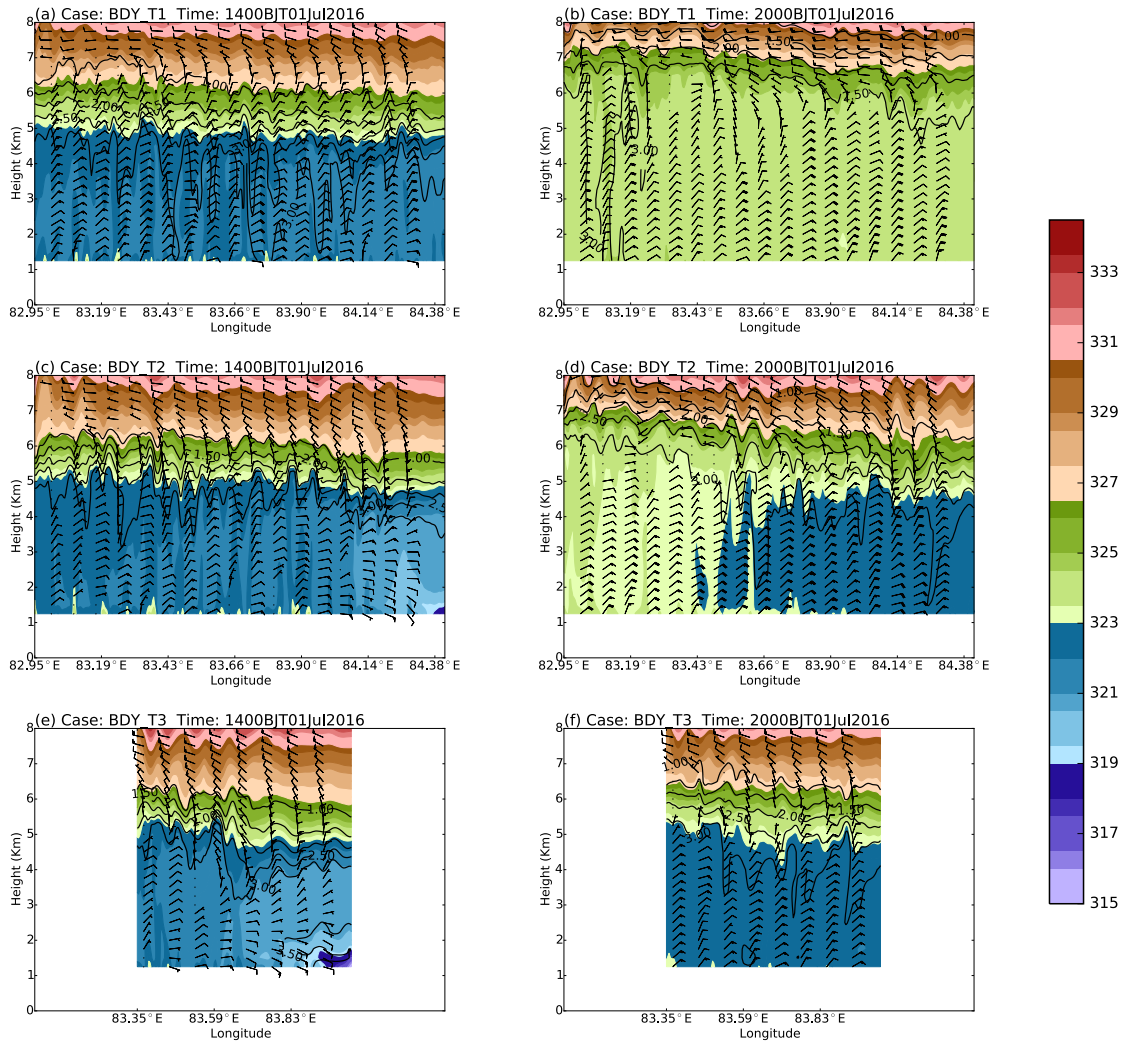
532 Figure 5 Vertical profiles of potential temperature (solid line, units: K) and vapor mixing

533 ratio(dash line, units: g/Kg)from innermost domain of simulations and observation of GPS

534 sounding at Tazhong station (83.63° E, 39.03° N) at (a)1100 (b) 1400 (c) 1700 (d) 2000 BJT

535 01 Jul2016. The profile of model output are averaged in a radius of 3.5km.

536



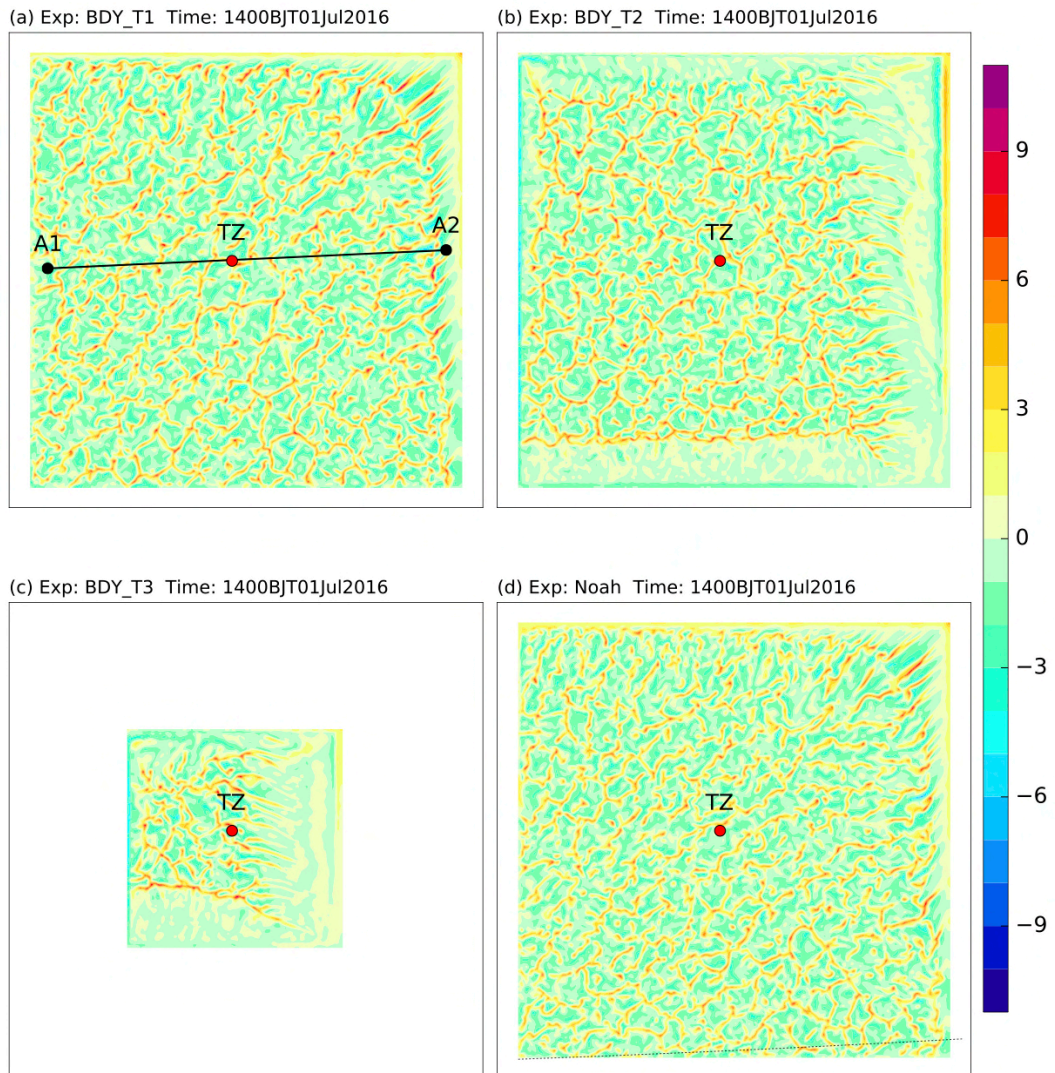
537

538 Figure 6 cross sections along 39.03°N of horizontal winds (barbs, units: m/s), at intervals of 5
 539 m/s, superposed with theta (shaded, units: K) and vapor mixing ratio(contour, units: g/Kg),
 540 from (a) BDY_T1, (c) BDY_T2, (e) BDY_T3 experiments at 1400 BJT 01JUL2016, (b), (d),
 541 (f) are the same as (a), (c), (e), but for 2000 BJT 01JUL2016.

542

543

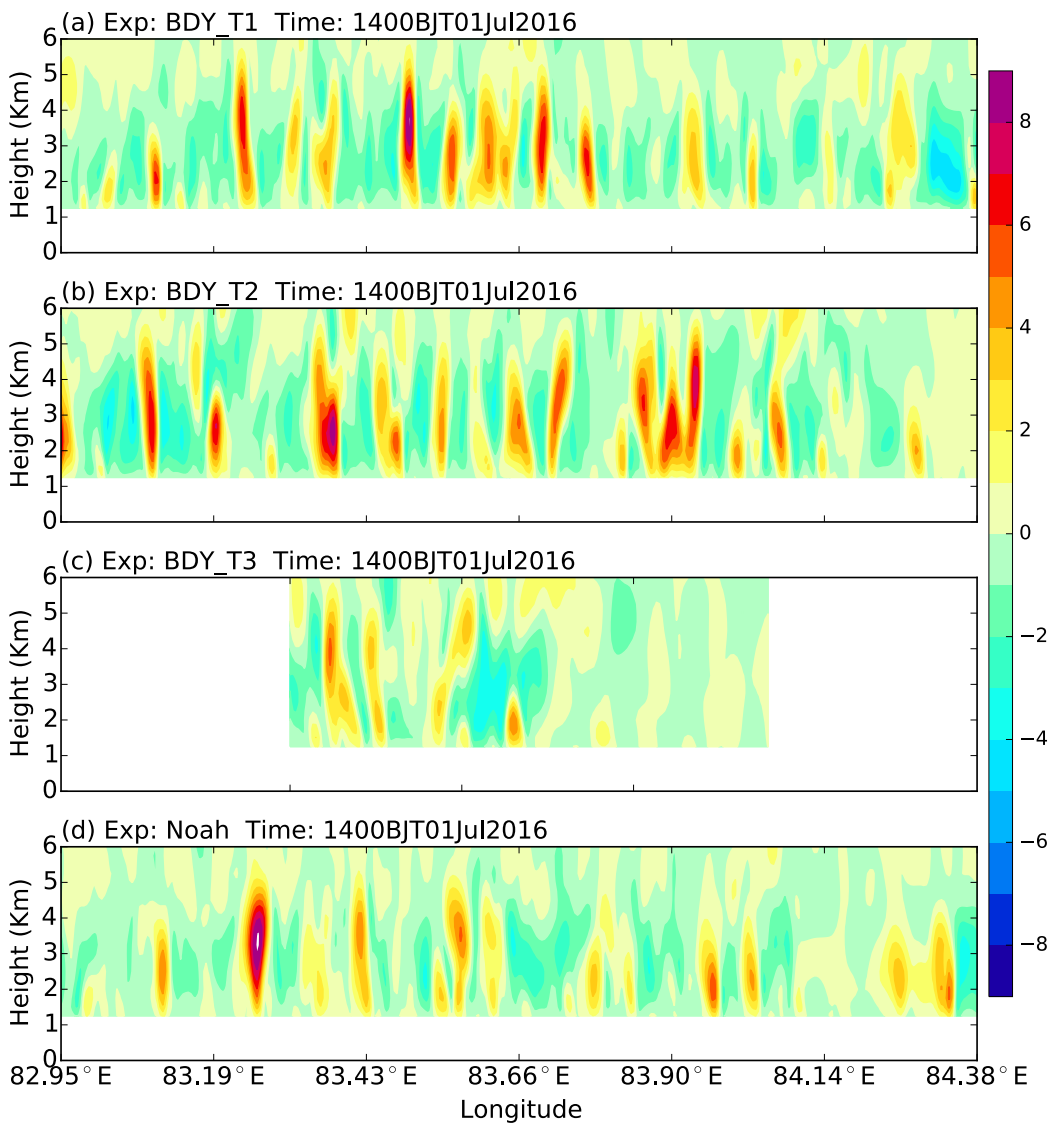
544



545

546 Figure 7 Instantaneous vertical velocity fields (shading: m/s) at 3000 m for (a) BDY_T1 (CTRL), (b)
 547 BDY_T2, (c) BDY_T3, and (d) Noah at 1400 BJT, 1 July 2016.

548



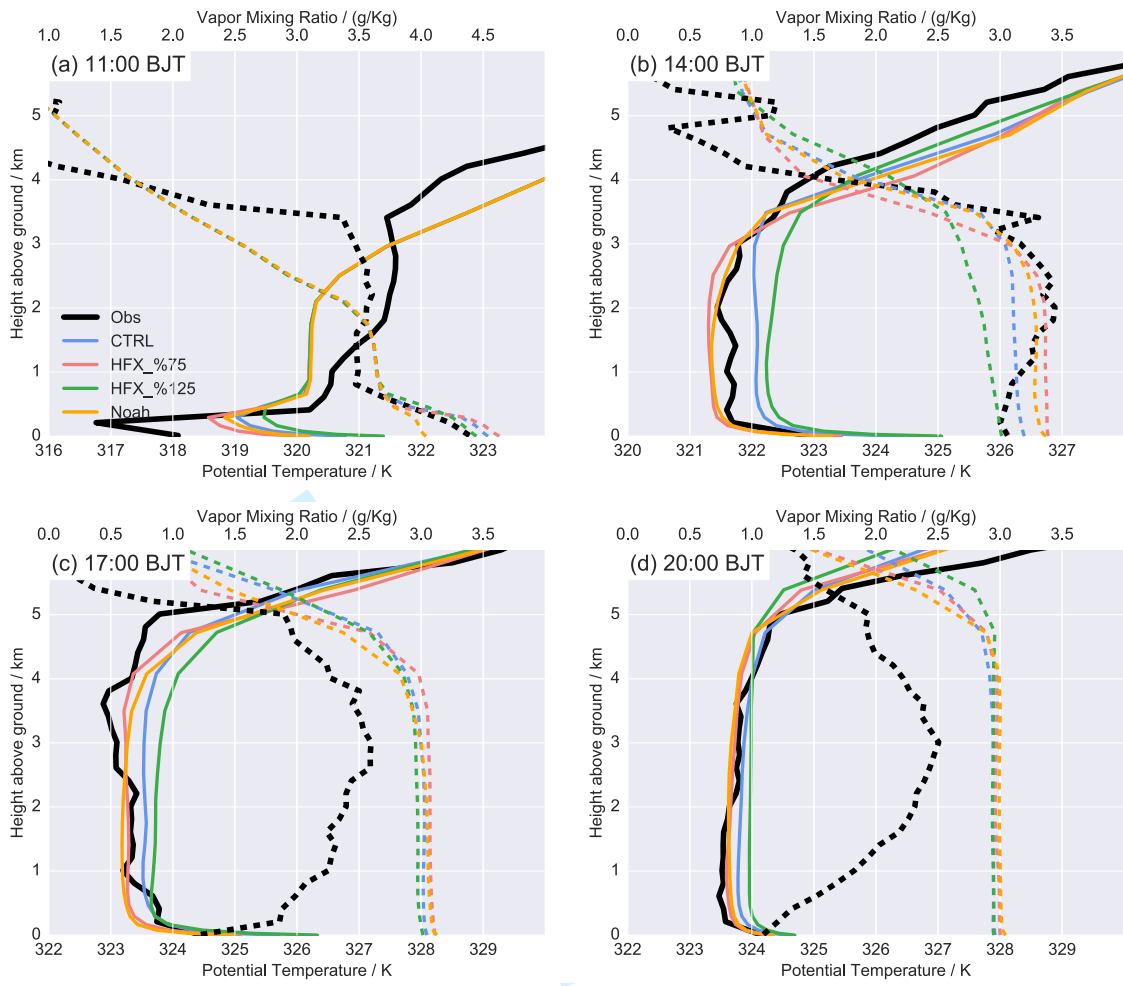
549

550 Figure 8 Vertical cross-section of instantaneous vertical velocity fields (shading: m/s) along
 551 A1-A2 in for for (a) BDY_T1 (CTRL), (b) BDY_T2, (c) BDY_T3, and (d) Noah at 1400 BJT, 1 July
 552 2016.

553

554

555

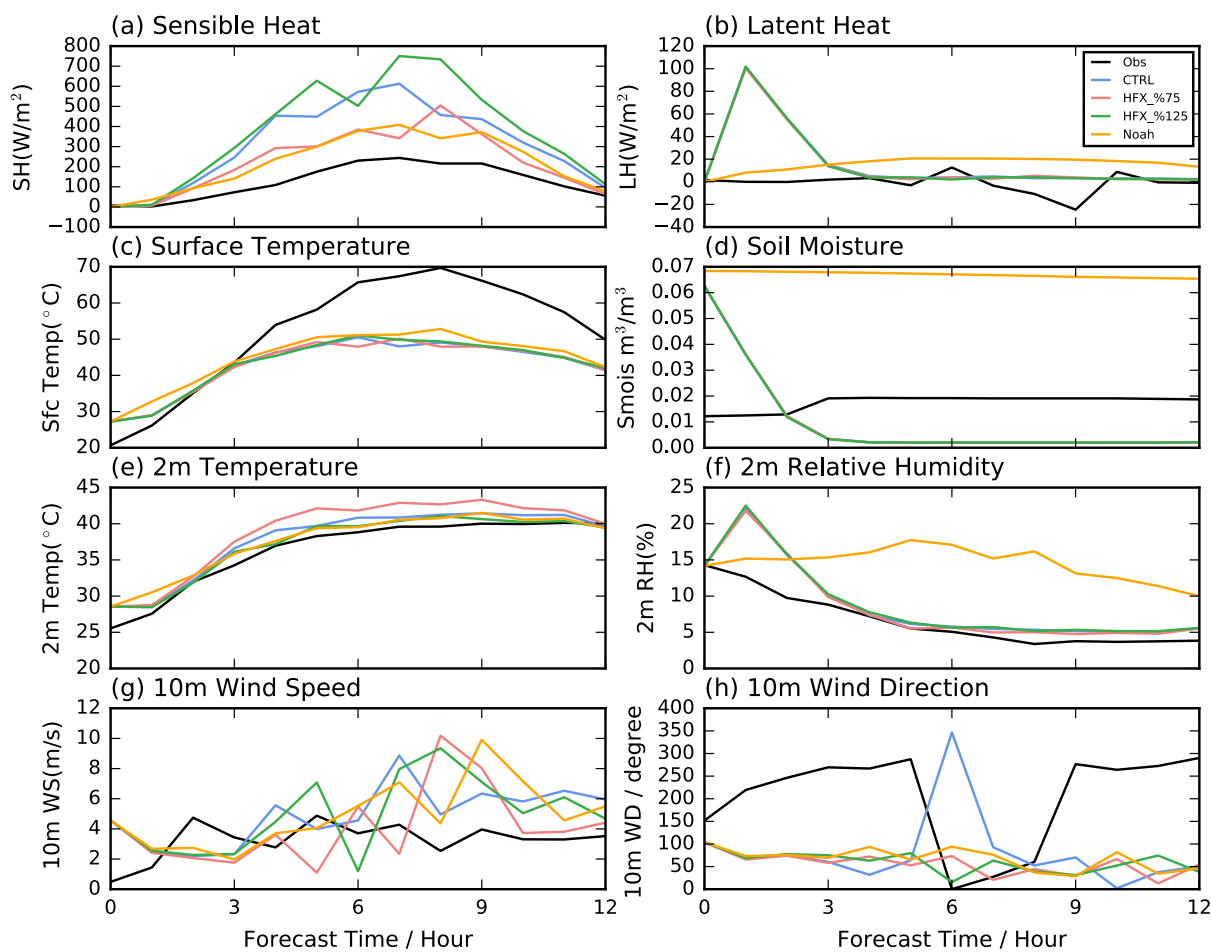


556

557

558

Figure 9 The same as Figure 5, but for SH flux sensitive and Noah land-surface experiment



559

560 Figure 10 The same as Figure 4, but for SH flux sensitive and Noah land-surface experiment.

561

562

Experiment	Name	Remarks
1	BDY_T1(CTRL)	LBC of D04 is provide by d03 every 1 hour with model grids 403x406
2	BDY_T2	As BDY_T1, but LBC of D04 is provide by d03 every 6 hour
3	BDY_T3	As BDY_T2, but with model grids 205 x 208.
4	HFX_%75	As CTRL_T2, but with SH 75%.
5	HFX_%125	As CTRL_T2, but with SH 125% .
6	Noah	As CTRL_T2, but with Noah surface-land model.

563

Table 1. List of designed experiments.

564

565

Variables	Sensible Heat		Latent Heat		Surface Temperature		Soil Moisture		2m Temperature		2m Relative Humidity		10m Wind Speed	
	RMSE	BIAS	RMSE	BIAS	RMSE	BIAS	RMSE	BIAS	RMSE	BIAS	RMSE	BIAS	RMSE	BIAS
Experiments														
CTRL	263.636	250.140	12.398	6.674	14.654	-13.373	0.017	-0.017	1.666	1.613	1.220	1.109	2.579	1.864
BDY_T2	249.395	240.660	12.383	6.253	14.116	-12.853	0.017	-0.017	1.912	1.817	1.275	1.162	2.943	1.307
BDY_T3	241.681	232.705	12.251	6.328	14.929	-13.737	0.017	-0.017	1.227	1.046	1.483	1.280	2.118	1.287
HFX_%75	151.119	134.594	12.544	6.354	14.740	-13.426	0.017	-0.017	3.078	3.016	0.956	0.826	3.335	0.874
HFX_%125	357.711	335.556	12.439	6.152	14.244	-13.043	0.017	-0.017	1.026	0.860	1.303	1.231	3.265	2.052
Noah	125.695	120.313	23.350	20.664	12.757	-11.502	0.048	0.048	1.046	0.983	10.116	9.904	2.788	1.795

566

567 Table 2. Summary of surface and air variables verification including integration hours from 3 to 12 h for Tazhong station.

568

569 **Reference:**

- 570 Chen, F., and J. Dudhia, 2001a: Coupling an Advanced Land Surface–Hydrology Model with the
571 Penn State–NCAR MM5 Modeling System. Part II: Preliminary Model Validation. *Monthly Weather*
572 *Review*, **129**, 587-604.
- 573 ———, 2001b: Coupling an advanced land surface-hydrology model with the Penn State-NCAR
574 MM5 modeling system. Part I: Model implementation and sensitivity. *Monthly Weather Review*,
575 **129**, 569-585.
- 576 Dudhia, J., 1989: Numerical study of convection observed during the winter monsoon experiment
577 using a mesoscale two-dimensional model. *J. Atmos. Sci.*, **46**, 3077-3107.
- 578 Engelstaedter, S., R. Washington, C. Flamant, D. J. Parker, C. J. T. Allen, and M. C. Todd, 2015: The
579 Saharan heat low and moisture transport pathways in the central Sahara—Multi-aircraft
580 observations and Africa-LAM evaluation. *Journal of Geophysical Research: Atmospheres*, **120**,
581 2015JD023123.
- 582 Garcia-Carreras, L., and Coauthors, 2015: The Turbulent Structure and Diurnal Growth of the
583 Saharan Atmospheric Boundary Layer. *Journal of the Atmospheric Sciences*, **72**, 693-713.
- 584 Han, B., S. Lü, and Y. Ao, 2012: Development of the convective boundary layer capping with a thick
585 neutral layer in Badanjilin: Observations and simulations. *Adv. Atmos. Sci.*, **29**, 177-192.
- 586 Heinold, B., P. Knippertz, and J. H. Marsham, 2013: Large Eddy Simulations of Nocturnal
587 Low-Level Jets over Desert Regions and Implications for Dust Emission. *EGU General Assembly*
588 *Conference*.
- 589 Heinold, B., P. Knippertz, and R. J. Beare, 2015: Idealized large-eddy simulations of nocturnal
590 low-level jets over subtropical desert regions and implications for dust-generating winds.
591 *Quarterly Journal of the Royal Meteorological Society*, **141**, 1740–1752.
- 592 Heinze, R., D. Mironov, and S. Raasch, 2015: Second-moment budgets in cloud topped boundary
593 layers: A large-eddy simulation study. *Journal of Advances in Modeling Earth Systems*, **7**, 510-536.
- 594 Hong, S.-Y., and H.-L. Pan, 1996: Nonlocal boundary layer vertical diffusion in a medium-range
595 forecast model. *Monthly weather review*, **124**, 2322-2339.
- 596 Hong, S.-Y., and J.-O. J. Lim, 2006: The WRF single-moment 6-class microphysics scheme (WSM6). *J.*
597 *Korean Meteor. Soc*, **42**, 129-151.
- 598 Hu, X.-M., J. W. Nielsen-Gammon, and F. Zhang, 2010: Evaluation of Three Planetary Boundary
599 Layer Schemes in the WRF Model. *Journal of Applied Meteorology and Climatology*, **49**,
600 1831-1844.
- 601 Kain, J. S., 1993: Convective parameterization for mesoscale models: The Kain-Fritsch scheme.
602 *The representation of cumulus convection in numerical models, Meteor. Monogr*, **46**, 165-170.
- 603 Kain, J. S., 2004: The Kain–Fritsch Convective Parameterization: An Update. *JOURNAL OF APPLIED*
604 *METEOROLOGY*, **43**, 170-181.
- 605 LeMone, M. A., M. Tewari, F. Chen, and J. Dudhia, 2013: Objectively Determined Fair-Weather CBL
606 Depths in the ARW-WRF Model and Their Comparison to CASES-97 Observations. *Monthly*
607 *Weather Review*, **141**, 30-54.
- 608 Liu, Y., Q. He, H. Zhang, and A. Mamtimin, 2012: Improving the CoLM in Taklimakan Desert
609 hinterland with accurate key parameters and an appropriate parameterization scheme. *Adv.*
610 *Atmos. Sci.*, **29**, 381-390.
- 611 Liu, Y., and Coauthors, 2011: Simultaneous nested modeling from the synoptic scale to the LES
612 scale for wind energy applications. *Journal of Wind Engineering and Industrial Aerodynamics*, **99**,

- 613 308-319.
- 614 Marsham, J. H., P. Knippertz, N. Dixon, D. J. Parker, and G. M. S. Lister, 2011: The importance of the
615 representation of deep convection for modeled dust - generating winds over West Africa during
616 summer. *Geophysical Research Letters*, **38**.
- 617 Mlawer, E. J., S. J. Taubman, P. D. Brown, M. J. Iacono, and S. A. Clough, 1997: Radiative transfer for
618 inhomogeneous atmospheres: RRTM, a validated correlated-k model for the longwave. *J. Geophys.*
619 *Res.*, **102**, 16663-16682.
- 620 Moeng, C.-H., J. Dudhia, J. Klemp, and P. Sullivan, 2007: Examining Two-Way Grid Nesting for Large
621 Eddy Simulation of the PBL Using the WRF Model. *Monthly Weather Review*, **135**, 2295-2311.
- 622 National Centers for Environmental Prediction, N. W. S. N. U. S. D. o. C., 2015: NCEP GDAS/FNL
623 0.25 Degree Global Tropospheric Analyses and Forecast Grids. Research Data Archive at the
624 National Center for Atmospheric Research, Computational and Information Systems Laboratory.
- 625 Rai, R. K., L. K. Berg, B. Kosović, J. D. Mirocha, M. S. Pekour, and W. J. Shaw, 2017: Comparison of
626 Measured and Numerically Simulated Turbulence Statistics in a Convective Boundary Layer Over
627 Complex Terrain. *Boundary-Layer Meteorology*, **163**, 69-89.
- 628 Schicker, I., D. Arnold Arias, and P. Seibert, 2016: Influences of updated land-use datasets on WRF
629 simulations for two Austrian regions. *Meteorology and Atmospheric Physics*, **128**, 279-301.
- 630 Shin, H. H., and S. Y. Hong, 2011: Intercomparison of Planetary Boundary-Layer Parametrizations
631 in the WRF Model for a Single Day from CASES-99. *Boundary-Layer Meteorology*, **139**, 261-281.
- 632 Shin, H. H., and S.-Y. Hong, 2015: Representation of the Subgrid-Scale Turbulent Transport in
633 Convective Boundary Layers at Gray-Zone Resolutions. *Monthly Weather Review*, **143**, 250-271.
- 634 Skamarock, W. C., and Coauthors, 2008: A Description of the Advanced Research WRF Version 3. .
635 *NCAR/TN-475+STR, NCAR TECHNICAL NOTE*.
- 636 Smirnova Tatiana, G., M. Brown John, G. Benjamin Stanley, and D. Kim, 2000: Parameterization of
637 cold - season processes in the MAPS land - surface scheme. *Journal of Geophysical Research:*
638 *Atmospheres*, **105**, 4077-4086.
- 639 Smirnova, T. G., J. M. Brown, and S. G. Benjamin, 1997: Performance of Different Soil Model
640 Configurations in Simulating Ground Surface Temperature and Surface Fluxes. *Monthly Weather*
641 *Review*, **125**, 1870-1884.
- 642 Stull, R. B., 1988: An Introduction to Boundary Layer Meteorology. *Atmospheric Sciences Library*, **8**,
643 89.
- 644 Sun, J., and Q. Xu, 2009: Parameterization of Sheared Convective Entrainment in the First-Order
645 Jump Model: Evaluation Through Large-Eddy Simulation. *Boundary-Layer Meteorology*, **132**,
646 279-288.
- 647 Talbot, C., E. Bou-Zeid, and J. Smith, 2012: Nested Mesoscale Large-Eddy Simulations with WRF:
648 Performance in Real Test Cases. *Journal of Hydrometeorology*, **13**, 1421-1441.
- 649 ter Maat, H. W., E. J. Moors, R. W. A. Hutjes, A. A. M. Holtslag, and A. J. Dolman, 2012: Exploring the
650 Impact of Land Cover and Topography on Rainfall Maxima in the Netherlands. *Journal of*
651 *Hydrometeorology*, **14**, 524-542.
- 652 WANG, and Coauthors, 2016a: Summer atmospheric boundary layer structure in the hinterland of
653 Taklimakan Desert, China. *Journal of Arid Land*, **8**, 846-860.
- 654 Wang, M., X. Xu, and H. Xu: The possible influence of the summertime deep atmospheric boundary
655 layer process over the Taklimakan Desert on the regional weather. (*submitted to Quarterly Journal*
656 *of the Royal Meteorological Society*).

- 657 Wang, M. Z., H. Lu, H. Ming, and J. Zhang, 2016b: Vertical structure of summer clear-sky
658 atmospheric boundary layer over the hinterland and southern margin of Taklamakan Desert: The
659 deep convective boundary layer of Taklamakan Desert. *Meteorological Applications*, **23**, 438-447.
- 660 Zhang, F., Z. Pu, and C. Wang, 2017: Effects of Boundary Layer Vertical Mixing on the Evolution of
661 Hurricanes over Land. *Monthly Weather Review*, **145**, 2343-2361.
- 662

For Review Only

Dear editors and reviewers,

We deeply appreciate the time and effort you've spent in reviewing our manuscript. Your comments are really thoughtful and helpful. Thus, we revised the manuscript, following your comments exactly. We have studied comments carefully and have made correction, which we hope meet with approval. Revised portion are marked in red in the paper. The main corrections in the paper and the responds to the reviewer's comments are as flowing:

Reviewer: 1

The paper is well written and presents works for PBL simulations using WRF framework. The authors explore the sensitivities of the model output due to lateral forcing of varying model sizes, frequency of the forcing, and surface heat flux. I would like the authors do some revisions on their manuscript. First, I have general comments here to address by the authors,

1. I encourage the author to reorganize the Method section as 2.1 Model configuration 2.2 Data 2.3 Synoptic

Thank you for the comments, we have reorganized the method section.

2. In Model configuration, please mention how long spin-up time was used. Did authors start all domains at same time? The authors also mention 51 vertical levels but you did not give what resolutions they are, particularly within the boundary layer. Please mention this.

Yes, we start all domains at same time. Height for lowest 20 levels are 1130.473, 1157.705, 1207.765, 1294.703, 1423.873, 1591.895, 1795.526, 2021.868, 2272.33, 2558.433, 2882.675, 3248.113, 3658.499, 4118.481, 4633.882, 5212.111, 5855.802, 6517.111, 7151.295, 7757.151.

3. The authors have presented several figures (vertical profiles and time series) but they have not mentioned how the plots are generated. Give details what the plots are representing – instantaneous or time/space averaged.

Thank you for the comments, we have added more details about profiles and series as follow:

Figure 4 Vertical profiles of potential temperature (solid line, units: K) and vapor mixing ratio(dash line, units: g/Kg)**from innermost domain of simulations and observation of GPS sounding at Tazhong station (83.63° E, 39.03° N)** at (a)1100 (b) 1400 (c) 1700 (d) 2000 BJT 01 Jul2016.

Figure 5 Time series of simulated surface **variables from innermost domain of simulations and surface observations at Tazhong station (83.63° E, 39.03° N)** initial at 0800 BJT 01July 2016 (a) sensible heat flux (W/m²), (b) latent heat flux(W/m²), (c) 2-m temperature (°C), (d) surface temperature (°C), (e) 2-m Relative Humidity(%) and (f) 10-m wind speed (m/s) with corresponding observations.

4. I guess the results from the innermost domain d04 are obtained without using perturbation near the inflow boundaries. It is not unexpected to see the difference in model output due to the varying grid size when the grid size reduces by more than half area. Similarly, more frequent forcing (1 hr) also provide more turbulence into the nested domain compared to 6 hr, as the model linearly interpolates tendencies between 6 hours. In this regard, it is always good to check how long fetch it took to develop the turbulence. Is the turbulence developed at the location where the model output is tapped? Have you checked results for other locations, may be far from the inflow boundaries where turbulence is well developed?

We have added instantaneous vertical velocity fields for the horizontal (Figure 7) and vertical cross-sections along Tazhong station (39°N) of vertical velocity(Figure 8).

The instantaneous vertical velocity fields for the horizontal are displayed in Figure 7. By 1400 BJT, the convection of CTRL simulation obviously intensified under strong surface heating (Xu et al. 2018). Thus, the maximum vertical velocity reaches 9 m/s and the depth of mixed layer grows to about 4.3 km (Figure 7 a). The distances between the boundary layer rolls correspondingly increase to about 12 km and the height of the peak updraughts is raised to just under 4 km. The cellular

shape of updrafts and downdrafts characteristic of boundary layer rolls is obvious in the horizontal view with the strength of convection. BDY_T2 and BDY_T3 experiments (Figure 7 b, c). both reproduce motions with much weaker maximum and minimum values at boundary of domain. In BDY_T3 experiment, Tazhong station at center of the model has been directly influenced by the inflow cold advection produced by low frequency LBCS and results in much weaker maximum and minimum value of w (about 6 m/s). However, despite the underestimate of potential temperature, the w fields for BDY_T2 experiment look similar to the CTRL w in plain view, and the horizontal extent of the updrafts/downdrafts agrees with the CTRL as can be inferred from Figure 7. To further examine the impact of LBCS on the simulation of desert CBL vertical cross-sections along Tazhong station (39°N) of vertical velocity are presented in Figure 8. Wide and regularly spaced updrafts along A1- A2 split into the stronger and more irregular motions in CTRL and BDY_T2. The updrafts are much weaker in the BDY_T3 experiment, as can be seen from Figure 8 c. Peak updrafts on BDY_T3 are about 4 m/s much weaker than on CTRL (9 m/s) and BDY_T2 (8 m/s). For BDY_T2 and BDY_T3, the distant of the inflow boundary is wider, and the intensity of the convection is weaker at the boundary. Compared with BDY_T2, the horizontal distribution of vertical velocity at Tazhong station in BDY_T3 experiments is much weaker.

5. I encouraged to run an additional simulation with different land-surface model as the authors mentioned that the heat flux and moisture quantities are playing the PBL growth.

Thank you for the comments, we have run an additional simulation with Noah land-surface model.

6. The authors tested with varying sensible heats in the simulation. I could not see the results of that in the manuscript. Could you present them together in figures 4-6 so that it helps reader to compare with other results?

Thank you for the comments and sorry for the mistake, Figure 8 and Figure 9 are the results from simulations with varying sensible heats. We have redrawn potential temperature and vapor mixing ratio into one figure. The new figure

also contains the results from Noah land-surface model as mentioned in comment 5.

7. In Fig. 7, I could not follow why the sizes of vertical cross-section is different between the panels in the first and the rest

Thank you for the comments and sorry for the mistake, we have reordered the Fig. 7(Figure 6 in the present manuscript), and modified BDY_T1 to BDY_T3. The sizes of vertical cross-section are different between the panels in BDY_T3 and the rest, because Sizes of BDY_T3 (205 X 208) is much smaller than the others(403X406).

8. I found cumbersome to go back and forth for the figures as the order of figures are random. Please put the figure in order. Similarly, the authors presented figures 8 and 9 in the list of figures, but I could not come across with those figures in the manuscript. Am I missing somewhere?

Thank you for the comments. We have reordered the figures. Figure 8 and Figure 9 are the results from simulations with varying sensible heats. Furthermore, we have put potential temperature and vapor mixing ratio into Figure 7.

9. When reading introduction, it looks like this work (desert case) is the first of its kind. Please make sure this. In addition, the authors may also mention complex terrain real case by Rai et al. (2017), where they did evaluate the turbulence statistics for the convective PBL in terms of turbulence model, domain size etc.

Thank you for the comments. We have cited the study, and changed the introduction.

Specific comments

1. Line 68: provide reference for ‘... 4-6 km during ...’.

Ok

2. Line 67 and 69: use either ABL or PBL and define it for the first time

Thank you for the comments. We have changed all ABL to PBL.

3. Line 129: why the section starts with 1, but not for introduction?

Thank you for the comments. We have changed introduction to the first section.

4. Line 144: define BJT

Thank you for the comments. We have changed BJT to BJT (Beijing Time)

5. Line 149-150: move to section model configuration

Ok

6. Line 164: make clear what is two experiments?

Thank you for the comments. We have changed 'Figure 1 shows the domain for two experiments.' to 'Figure 1 shows the domain for all experiments except for BDY_T3. Smaller grid sizes (205 x 208) are used in experiment BDY_T3 to verify the effect of domain size on LES simulation.'

7. Line 173: use space in '... millibars(National'. Check this throughout the manuscript as I found they occurs everywhere.

Ok

8. Line 185-186: check sentence syntax for 'For one-way nest, ...'

Thank you for the comments. We have changed 'For one-way nest, Specified LBC obtained from coarser model simulation.' to 'For one-way nest, specified LBC is obtained from coarser model simulation.'

9. Line 218: define SH

We have change 'SH' to 'SH (surface sensible heat flux)'

10. Line 245: see the period

Ok.

11. Line 279: it to It?

Ok.

12. Line 341-342: check the sentence syntax

Ok.

13. Line 351: the to The?

Ok.

Reviewer: 2

General comments

Characteristics of the convective boundary layer (CBL) over desert(s) are not

well defined due to lacking of observational data and high resolution numerical simulations. It definitely represents one of the research interests for the atmospheric boundary layer meteorology, weather, and climate. In this manuscript, the authors attempted to present the performance of WRF/LES on simulating the CBL structures and their evolution over the Taklimakan Desert during the summer daytime. They presented how the simulated vertical profiles of potential temperature and specific humidity were sensitive to the ingest frequency of lateral boundary conditions, and how the on simulated vertical profiles changed with surface heat fluxes. It is not surprised that the WRF/LES simulations with hourly update of lateral boundary conditions ingest showed better agreement with the observations (see Figure 4.b). The findings obtained from these two group sensitivity studies are not new at all. As indicated by the manuscript title, the study is supposed to focus on the performance of WRF/Chem. No enough meaningful evaluation results are provided in the manuscript to support the objective indicated by the manuscript title. The manuscript structure isn't well designed. Scientific questions are not clearly defined and insightful analyses are lacking. Extensive grammar errors make the manuscript very difficult to read and understand. No significant results were obtained from this study. Therefore, the manuscript is suggested to reject given the current status.

Major comments

1. Observation-simulation comparisons (e.g., time series and vertical profiles) and statistical evaluations of the model simulation (considered as a base case) should be presented before the sensitivity studies (sections 3.1 and 3.2).

Thank you for the comment. We have reordered the section 3.1 and section 3.2.

2. How are the lateral boundary conditions of the innermost domain

updated during the simulations? Is it not updated every integration time step? It is not useful to present sensitivity studies on impact of updated frequency of lateral boundary layer conditions on the WRF/LES results.

Thank you for the comments. We conducted one-way nest WRF from mesoscale down to LES-scales. For one-way nest, Specified LBC is obtained from coarser model simulation. For innermost, all forecast times from d03 simulation are used to specify the LBC. Limited by storage of our supercomputer, all model results are in 1hour interval.

As in Talbot et al. (2012), LES model fields are primarily influenced by their mesoscale meteorological forcing. Thus, in this study, we want to further examine the impact of uncertainties of LBC on LES simulation. The results suggest that the model results are sensitive to changes in time resolution and domain size of Specified LBC. The mismatch among sensitive experiments is present means that the effect of LBC needs to be quantified to realize a more realistic performance in the sub-kilometer simulations.

3. Why the vertical profiles of specific humidity (Figure 5) are very different from those of potential temperature (Figure 4) within the CBL. Is this the real case? What are the main reasons causing such type of vertical distribution?

Yes, it's the real case. We also find inverse humidity in July 2017. Inverse humidity may be caused by the joint of the heterogeneous humidity Pattern and Large-scale advection over the underlying surface. For instance, interaction of oasis with desert environment may resulted in the inverse humidity layer in desert PBL.

4. Why is the maximum observed surface sensible heat flux less than 250 W·m⁻²? This is not consistent with the boundary layer height (up to 5000 m). Is it possible to observe such low sensible heat flux over the desert?

Thank you for the comments,

(1) it should be noted that the SH and LH based on eddy correlation might be underestimated. Researchers found that if the other two terms in the budget—net radiation and flux into the soil were accurate, used data for the whole experiment to find the $H + LE$ are equal to an average of 75% of what would be required for balancing the surface energy budget (LeMone et al. 2013). Under this scenario, the government would soon recoup its investment and the debt pile would shrink.

(2) RL (residual layer) may play a key role in the deep PBL at Taklimakan desert. At 1100 BJT, when the PBLH was about 300 m in observation as shown above, potential temperature in the PBL were about 317 K in PBL and 320 K in RL, respectively. When the potential temperature in CBL increased to 320 K because of heating from under layer surface, the CBL merged with the RL, and the height of PBL reached 3000m in the observations at 1400 BJT. These results are in good agreement with Han et al. (2012). By analysis of observation of a CBL in the Badanjilin region, they found a rapid development process of CBL after 1200 LST, which appeared to be a jump of PBLH when the inversion layer vanished.

(3) Results of simulations on desert PBL in the morning agree with the previous studies of sensitivities land-surface model for other areas (Hu et al. 2010; Zhang et al. 2017). However, during 1700~2000 BJT 01July (Figure 9b, d), all experiments produce nearly the same CBLH and moisture in agreement with observation in the PBL. The effects of SH on the evolution of Taklimakan PBL structures during this period are needed to be further examined and discussed. So, the question is: why are simulations insensitive to land-surface process by the end of the day? As in Stull (1988), the development of CBL is mainly influenced by the effect of thermodynamic and turbulent entrainment without considering large scale factors such as large scale advection or subsidence. Besides the surface sensible heat, the intensity of entrainment process determines the increasing rate of CBL. Thus, the entrainment rate w_e is a valuable indicator for the development of PBL structure.

The rate of growth of the convective boundary layer is mainly determined by the entrainment rate w_e at the inversion layer without considering large scale

vertical motion. w_e usually has a positive correlation with heat flux amount at the inversion layer $\overline{(w'\theta_v)'}_h$, and large LES experiments show $\overline{(w'\theta_v)'}_h$ is about 0.2 times the surface flux of buoyancy $\overline{(w'\theta_0)'}_s$. During the period from 1100 to 1400 BJT, larger SH is obviously correlated with stronger turbulent entrainment and warmer air from free atmosphere (FA) entraining into ML. As a result, CBL develop rapidly and is warm too fast in the early simulation phase due to the obviously increasing temperature and strong vertical mixing in model. Of interesting is that reduction in SH reproduces better desert PBL evolution in the early simulation phase, as $SH-75\%$ and Noah produce the smallest simulation errors in both temperature and moisture. However, one should note that CBLH and potential temperature for $SH-75\%$ and Noah have reached above 5000 m and 323.2 K respectively at 1700 BJT (Figure 9a). For the rest of the day, the increase rate of CBL height slows down due to the deep CBL(>5000m) which require more heat for the growth of PBL depth; Moreover, w_e decrease with increasing inversion intensity, which inhibits the mixing and entrainment processes. These two factors obviously limit the growth of CBL when CBLH is over 5000 m in this deep desert CBL case. Therefore, increasing SH from 75% to 125% significantly reduce the total time needed for CBL increase to a relative low altitude (< 5 km) at the middle and preliminary stage of the development of CBL rather than produce higher CBL at the late stage. When height of CBL over Taklimakan desert exceeds 5000 m, it might not change with proportion to SH fluxes (Figure 9d). As a result, PBL of WRF simulations are basically the same, and not sensitive to SH fluxes by the end of the day.

5. It is required to calculate statistical parameters for the model evaluation.

Thank you for your comments, we have added 'Summary of surface and air variables verification including integration hours from 3 to 12 h for Tazhong station.' in Table 2.

6. L206-207: How the more frequently LBCs may cause the cold advection?

Sorry for the mistake, we have changed 'The more frequently updated LBC is

desirable to cold zone near the LBC, which results in cold advection of the temperature and moisture to the area of interest' to 'The lower frequently updated LBC is desirable to cold zone near the LBC, which results in cold advection of the temperature and moisture to the area of interest'.

Lower frequently LBCs may cause the cold advection, because earlier model results from d03 simulation are used to specify the LBC, which. In this case, BDY_T2 and BDY_T3 experiment LBC with 6 interval results from D03 produced cold zone in the lateral boundaries, and resulted in the cold advection.

7. The authors pointed out that the soil moisture was over-estimated by the model and initial soil moisture is higher than the observations (see L242-243, L248-250). If this is the case, the sensible could be under-predicted. However, the simulation results show the over-prediction of sensible heat flux by the model (see L218-220).

Thank you for the comments. Yes, the large overestimate of soil moisture makes LH (Figure4 b, f) from the model continue to increase. As a result, near-surface of model is far moister than that of observation at the first few hours of model integration. However, an interesting result to be note is that the model simulation has the abilities to correct some of the bias due to the initial condition of the surface; The results from CTRL experiment are closer to observation after 3 hours' spin-up. Thus, the large overestimate of soil moisture at initial stage(0~3hours) may have little impact on the large over-prediction of sensible heat flux during 3~9 hours' simulation.

8. As pointed out by the authors that the surface heat flux is the main driving force to the boundary layer growth. The model captured the boundary layer height quite well (see the control case in Figure 4.d) even the surface heat flux is significantly over-predicted by the model (see Figure 6).

Results of simulations on desert PBL in the morning agree with the previous studies of sensitivities land-surface model for other areas (Hu et al. 2010; Zhang et al. 2017). However, during 1700~2000 BJT 01July (Figure 9b, d), all experiments produce nearly the same CBLH and moisture in agreement with observation in the

PBL. The effects of SH on the evolution of Taklimakan PBL structures during this period are needed to be further examined and discussed. So, the question is: why are simulations insensitive to land-surface process by the end of the day? As in Stull (1988), the development of CBL is mainly influenced by the effect of thermodynamic and turbulent entrainment without considering large scale factors such as large scale advection or subsidence. Besides the surface sensible heat, the intensity of entrainment process determines the increasing rate of CBL. Thus, the entrainment rate w_e is a valuable indicator for the development of PBL structure.

The rate of growth of the convective boundary layer is mainly determined by the entrainment rate w_e at the inversion layer without considering large scale vertical motion. w_e usually has a positive correlation with heat flux amount at the inversion layer $\overline{(w'\theta_v)'}_h$, and large LES experiments show $\overline{(w'\theta_v)'}_h$ is about 0.2 times the surface flux of buoyancy $\overline{(w'\theta_0)'}$. During the period from 1100 to 1400 BJT, larger SH is obviously correlated with stronger turbulent entrainment and warmer air from free atmosphere (FA) entraining into ML. As a result, CBL develop rapidly and is warm too fast in the early simulation phase due to the obviously increasing temperature and strong vertical mixing in model. Of interesting is that reduction in SH reproduces better desert PBL evolution in the early simulation phase, as SH-75% and Noah produce the smallest simulation errors in both temperature and moisture. However, one should note that CBLH and potential temperature for SH-75% and Noah have reached above 5000 m and 323.2 K respectively at 1700 BJT (Figure 9a). For the rest of the day, the increase rate of CBL height slows down due to the deep CBL(>5000m) which require more heat for the growth of PBL depth; Moreover, w_e decrease with increasing inversion intensity, which inhibits the mixing and entrainment processes. These two factors obviously limit the growth of CBL when CBLH is over 5000 m in this deep desert CBL case. Therefore, increasing SH from 75% to 125% significantly reduce the total time needed for CBL increase to a relative low altitude (< 5 km) at the middle and preliminary stage of the development of CBL rather than produce higher CBL at the late stage. When height of CBL over

Taklimakan desert exceeds 5000 m, it might not change with proportion to SH fluxes (Figure 9d). As a result, PBL of WRF simulations are basically the same, and not sensitive to SH fluxes by the end of the day.

9. Entrainment process could play an important role in the CBL development over the Desert. However, it hasn't discussed by the authors.

As in comment 8.

10. There are too many grammar errors throughout the manuscript. It is difficult to list all the errors here.

We have carefully revised the manuscript according to the reviewers' comments, and also have rescrutinized to improve the English by a native English speaker.

Reviewer: 3

Major comments

1 Observation

The observation site is located in the center of desert. As the author says, the PBL there can reach 5000 m. Is this conclusion just based on the observation results given in fig.4 and 5? Or this results has been mentioned in other study from more atmospheric profiles? In my opinion, profiles only in one day cannot represent the common structures of low atmosphere as well as PBL. To state that the PBL in this desert can reach 5000 m frequently instead of occasionally, more profiles need to be given. Maybe the author can found some other similar research to support their conclusion.

The conclusion of desert PBL can reach 5000 m is based on the study of Wang et.al. They states the PBL height of Tazhong and four surrounding stations (Minfeng, Korla, Ruoqiang and Kashgar, Figure b1) during July 2016. The number of days when

the ABL exceeds 4,000 m depth is 8, 9, 5, 4 and 2 respectively, and that of higher than 3,000 m is 20, 22, 13, 15, and 5 respectively.

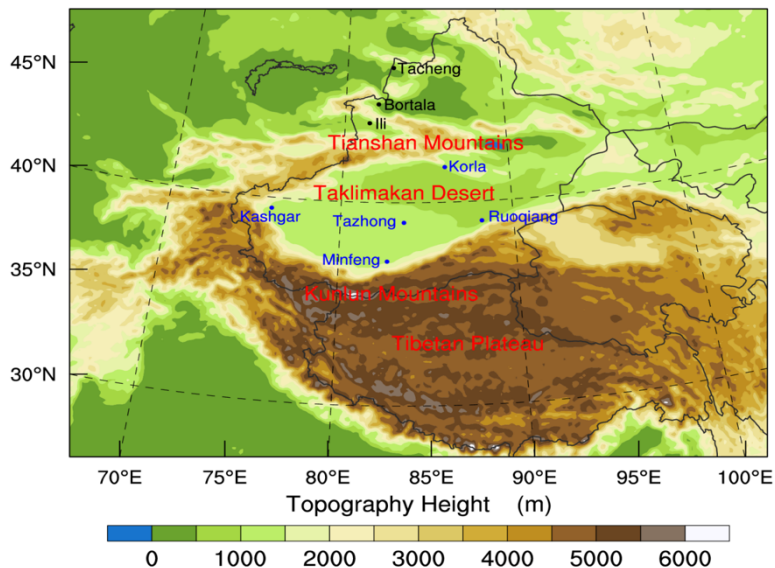


Figure b1. Location of the sounding stations.

Table 3. The number of days with deep boundary layers in the hinterland and the surrounding areas of the Taklimakan Desert in July 2016.

Height of the boundary layer	Tazhong	Minfeng	Korla	Ruoqiang	Karshgar
≥5000 m	1	1	1	1	0
≥4000 m	8	9	5	4	2
≥3500 m	15	17	6	9	4
≥3000 m	20	22	13	15	5

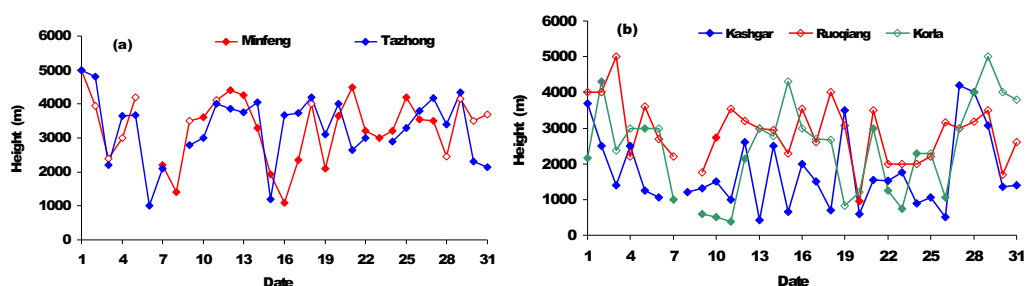


Figure b2. Curves of the daily height variations of the boundary layers in the hinterland and the surrounding areas of the Taklimakan Desert at 19:15 in July 2016.

(The solid symbols representing the height of the convective boundary layer while the hollow symbols representing the height of the residual mixed layer)

2 WRF-LES

The author compare the results from WRF-LES to that from radio sounder. It should be noted that the radiosounder also floated horizontally during its raising. The distance of horizontal displacement, generally 1-30 km if the radiosounder can reach 20 km high, depend on the horizontal wind. The horizontal movement can be ignored if the grid size of numerical model is larger than 20 km, but as for this study, the grid size is 330m, the effect of horizontal movement should be state in this study.

Yes, when radio-sounder reach 6km height, it floating about 7Km away. Thus, for more accuracy, we have averaged the profile of model output center at Tazhong station in 3.5km radius.

The author should also state why choosing WRF-LES, instead of LES or one-dimension PBL model, in study.

Thank you for the comment.

(1) As in Xu et al. (2018), we have examined impact of PBL schemes on simulating deep PBL over Taklimakan dessert. Results show that there are still uncertainties, despite of using the state-of-the-art scale dependencies PBL scheme with reference data from LES.

(2) The aim of this paper is to examine assess the skillfulness of WRF-LES in relative coarse resolution (333m) over Taklimakan dessert, in simulating real cases of desert PBL process during boreal summer events in Taklimakan.

WRF-LES can give the 3-D structure of lower atmosphere, but I note only fig.7 shows such results, and the corresponding statement in the manuscript seems contributed little to the main conclusion. I suggested that the authors add some discussion on the horizontal distribution of PBL or lapse rate of lower atmosphere over the desert region, and given a detailed description on the effect of advection in the night before the day of radio sound launched. By doing this, the difference in initial profile between observation and simulation may be better understand.

Thank you for the comment. We have added instantaneous vertical velocity fields for the horizontal (Figure 7) and vertical cross-sections along Tazhong station (39° N) of vertical velocity (Figure 8).

The instantaneous vertical velocity fields for the horizontal are displayed in Figure 7. By 1400 BJT, the convection of WRF-LES simulation obviously intensified under strong surface heating (Xu et al. 2018). Thus, the maximum vertical velocity reaches 9 m/s and the depth of mixed layer grows to about 4.3 km (Figure 7 a). The distances between the boundary layer rolls correspondingly increase to about 12 km and the height of the peak updrafts is raised to just under 4 km. The cellular shape of updrafts and downdrafts characteristic of boundary layer rolls is obvious in the horizontal view with the strength of convection. BDY_T2 and BDY_T3 experiments (Figure 7 b, c), both reproduce motions with much weaker maximum and minimum values at boundary of domain. In BDY_T3 experiment, Tazhong station at center of the model has been directly influenced by the inflow cold advection produced by low frequency LBCS and results in much weaker maximum and minimum value of (about 6 m/s). However, despite the underestimate of potential temperature, the fields for BDY_T2 experiment look similar to the CTRL in plain view, and the horizontal extent of the updrafts/downdrafts agrees with the CTRL as can be inferred from Figure 7. To further examine the impact of LBCS on the simulation of desert CBL vertical cross-sections along Tazhong station (39° N) of vertical velocity are presented in Figure 8. Wide and regularly spaced updrafts along A1-A2 split into the stronger and more irregular motions in CTRL and BDY_T2. The updrafts are much weaker in the BDY_T3 experiment, as can be seen from Figure 8 c. Peak updrafts on BDY_T3 are about 4 m/s much weaker than on CTRL (9 m/s) and BDY_T2 (8 m/s). For BDY_T2 and BDY_T3, the distant of the inflow boundary is wider, and the intensity of the convection is weaker at the boundary. Compared with BDY_T2, the horizontal distribution of vertical velocity at Tazhong station in BDY_T3 experiments is much weaker.

3 Land surface model

The difference in surface flux between simulation and observation seems to be too large, especially for the sensible heat flux (SH). The peak SH is about 250 Wm^{-2} , but all simulations give the peak SH to be $\sim 600 \text{ Wm}^{-2}$. As the author mentioned, SH is a key factor to the development of convective boundary layer. If the land surface model give a similar SH as observed, is the 5000 m high PBL can still be given in all simulation cases? If not/so, why? Did the author verified all crucial parameterization schemes (like PBL, LSM etc.) before all simulations start? I also noted the simulated latent heat flux is also greater than the observed one, which infers the net radiation at land surface might be overestimated too. The author mentioned the USGS land use data might be problematic, but no detailed information has been given. For example, is the albedo between observation and simulation comparable? Only if the surface parameters and process are properly given, the PBL process, which is a combination of land surface process and free atmosphere dynamic processes, in numerical model can be more sound and meaningful.

If the land surface model give a similar SH as observed, is the 5000 m high PBL can still be given in all simulation cases? If not/so, why?

Results of simulations on desert PBL in the morning agree with the previous studies of sensitivities land-surface model for other areas (Hu et al. 2010; Zhang et al. 2017). However, during 1700~2000 BJT 01July (Figure 9b, d), all experiments produce nearly the same CBLH and moisture in agreement with observation in the PBL. The effects of SH on the evolution of Taklimakan PBL structures during this period are needed to be further examined and discussed. So, the question is: why are simulations insensitive to land-surface process by the end of the day? As in Stull (1988), the development of CBL is mainly influenced by the effect of thermodynamic and turbulent entrainment without considering large scale factors such as large scale advection or subsidence. Besides the surface sensible heat, the intensity of entrainment process determines the increasing rate of CBL. Thus, the entrainment rate w_e is a valuable indicator for the development of PBL structure.

The rate of growth of the convective boundary layer is mainly determined by the entrainment rate w_e at the inversion layer without considering large scale vertical motion. w_e usually has a positive correlation with heat flux amount at the inversion layer $\overline{(w'\theta_v')_h}$, and large LES experiments show $\overline{(w'\theta_v')_h}$ is about 0.2 times the

surface flux of buoyancy $\overline{(w'\theta_0')}$. During the period from 1100 to 1400 BJT, larger SH is obviously correlated with stronger turbulent entrainment and warmer air from free atmosphere (FA) entraining into ML. As a result, CBL develop rapidly and is warm too fast in the early simulation phase due to the obviously increasing temperature and strong vertical mixing in model. Of interesting is that reduction in SH reproduces better desert PBL evolution in the early simulation phase, as SH-75% and Noah produce the smallest simulation errors in both temperature and moisture. However, one should note that CBLH and potential temperature for SH-75% and Noah have reached above 5000 m and 323.2 K respectively at 1700 BJT (Figure 9a). For the rest of the day, the increase rate of CBL height slows down due to the deep CBL(>5000m) which require more heat for the growth of PBL depth; Moreover, w_e decrease with increasing inversion intensity, which inhibits the mixing and entrainment processes. These two factors obviously limit the growth of CBL when CBLH is over 5000 m in this deep desert CBL case. Therefore, increasing SH from 75% to 125% significantly reduce the total time needed for CBL increase to a relative low altitude (< 5 km) at the middle and preliminary stage of the development of CBL rather than produce higher CBL at the late stage. When height of CBL over Taklimakan desert exceeds 5000 m, it might not change with proportion to SH fluxes (Figure 9d). As a result, PBL of WRF simulations are basically the same, and not sensitive to SH fluxes by the end of the day.

Did the author verified all crucial parameterization schemes (like PBL, LSM etc.) before all simulations start? I also noted the simulated latent heat flux is also greater than the observed one, which infers the net radiation at land surface might be overestimated too. The author mentioned the USGS land use data might be problematic, but no detailed information has been given. For example, is the albedo between observation and simulation comparable? Only if the surface parameters and process are properly given, the PBL process, which is a combination of land surface process and free atmosphere dynamic processes, in numerical model can be more sound and meaningful.

(1) Yes, we have verified PBL parameterization schemes. As in Xu et al. (2018), we have verified impact of different PBL schemes on the same case as this study.

(2) We also added an experiment with Noah LSM to be compare to the RUC LSM used in CTRL experiment.

(3) To verify the influence of landuse on overestimate of SH, the albedo of observation is calculated from upward show wave radiation and downward. Results show that albedo from observation (0.239) is in agreement with that of CTRL (0.21) experiment. This indicates that difference of landuse between model and observation are not the key reason for overestimate of SH.

(4) However, One possible reason for inverse humidity may be caused by the error in landuse. Inverse humidity may be caused by the joint of the heterogeneous humidity Pattern and Large-scale advection over the underlying surface. For instance, interaction of oasis with desert environment may resulted in the inverse humidity layer in desert PBL.

4 Conclusions

One of the main conclusion is that the surface sensible flux is essential to the simulation of PBL, which is a common realization of PBL development because the buoyancy flux is main forcing of convective boundary layer rather than wind shear. However, from the sensitive experiment, when SH changed significantly, the shape of atmospheric profile did not show similar magnitude of change, and I guess the height of PBL did not increase/decrease for 25% (the author mentioned the change of PBL height should be 15% in Abstract, but I cannot found similar statement in section 3.3). How the height of PBL were defined should also be given in the manuscript. I noted that the residual layer at 1100 BJT is neutral and deep, is it the main reason for the deep PBL instead of SH? The author can refer to the work of Han in AAS in 2012.

Yes, RL(residual layer) may play a key role in the deep PBL.

(1) One should note that RL (residual layer) play a key role in the deep PBL at Taklimakan desert. At 1100 BJT, when the PBLH was about 300 m in observation as show above, potential temperature in the were about 317 in PBL and 320 K in RL, respectively. When the potential temperature in CBL increased to 320 K because of

heating from under layer surface, the CBL merged with the RL, and the height of PBL reach 3000m in the observations at 1400 BJT. These results are in good agreement with Han et al. (2012). By analysis of observation of a CBL in the Badanjilin region, they found a rapid development process of CBL after 1200 LST, which appeared to be a jump of PBLH when the inversion layer vanished.

(2) As in comment 4. The rate of growth of the convective boundary layer is mainly determined by the entrainment rate w_e at the inversion layer without considering large scale vertical motion. w_e usually has a positive correlation with heat flux amount at the inversion layer $\overline{(w'\theta_v)'}_h$, and large LES experiments show $\overline{(w'\theta_v)'}_h$ is about 0.2 times the surface flux of buoyancy $\overline{(w'\theta_0)'}$. During the period from 1100 to 1400 BJT, larger SH is obviously correlated with stronger turbulent entrainment and warmer air from free atmosphere (FA) entraining into ML. As a result, CBL develop rapidly and is warm too fast in the early simulation phase due to the obviously increasing temperature and strong vertical mixing in model. Of interesting is that reduction in SH reproduces better desert PBL evolution in the early simulation phase, as $SH-75\%$ and Noah produce the smallest simulation errors in both temperature and moisture. However, one should note that CBLH and potential temperature for $SH-75\%$ and Noah have reached above 5000 m and 323.2 K respectively at 1700 BJT (Figure 9a). For the rest of the day, the increase rate of CBL height slows down due to the deep CBL(>5000m) which require more heat for the growth of PBL depth; Moreover, w_e decrease with increasing inversion intensity, which inhibits the mixing and entrainment processes. These two factors obviously limit the growth of CBL when CBLH is over 5000 m in this deep desert CBL case. Therefore, increasing SH from 75% to 125% significantly reduce the total time needed for CBL increase to a relative low altitude (< 5 km) at the middle and preliminary stage of the development of CBL rather than produce higher CBL at the late stage. When height of CBL over Taklimakan desert exceeds 5000 m, it might not change with proportion to SH fluxes (Figure 9d). As a result, PBL of WRF

simulations are basically the same, and not sensitive to SH fluxes by the end of the day.

Minor comments

Some statements may confuse the readers, I listed them below.

1 P4L91" ... mesoscale atmospheric models are still cannot..."; -> unable to?

Ok, we have changed 'still cannot' to 'still unable to'.

2 P6L136 "The high-pressure system at low level, which is termed of heat low (Figure 3)," is this system high pressure or not?

We have changed "The high-pressure system at low level, which is termed of heat low (Figure 3)," to "The low-pressure system at low level, which is termed of heat low (Figure 3),"

Editor(s)' Comments to Author:

Editor: 1

Comments to the Author:

I have thought long-and-hard about this work since the reviews were so disparate (one reviewer suggested rejection). So I urge you to strongly consider carefully addressing the comments, particularly better examining the importance of land-surface processes and entrainment, as well as improving writing.

Ok

The 1st reviewer encouraged more sensitivity simulations and investigation, particularly in terms of importance of land-surface processes and inflow fetch. Also the reviewer raised a lot of issue in terms of writing! Please be very careful and make sure present your results nicely!

Ok

The 2nd reviewer is most critical. He suggested more examination of role of land surface fluxes and entrainment process on the development of CBL. Actually the 3rd reviewer suggested the same issue (e.g., importance of residual layer is nearly equivalent as the importance of entrainment in terms of CBL development). BTW, a lot of existing papers discussed the entrainment, which should be cited.

Also the 2nd reviewer pointed out the writing of the manuscript needs significant improvement, including organization, introduction, and grammar.

Ok

The 3rd reviewer suggested more discussion, particularly importance of land surface processes/fluxes on the development of PBL, as well as the role of pre-existing residual layer, and impact of horizontal drifting of the sounds.

Ok

Please put profiles of potential temperature and water vapor mixing ratio side by side since they can collectively indicate the boundary layer structure, that is, combine Figures 4 & 5; Figures 8&9

Thank you for your comments, We have redraw Figures 4 & 5 and Figures 8&9 into Figure 5 and Figure 7 respectively.

Reference

- Hu, X.-M., J. W. Nielsen-Gammon, and F. Zhang, 2010: Evaluation of Three Planetary Boundary Layer Schemes in the WRF Model. *Journal of Applied Meteorology and Climatology*, **49**, 1831-1844.
- LeMone, M. A., M. Tewari, F. Chen, and J. Dudhia, 2013: Objectively Determined Fair-Weather CBL Depths in the ARW-WRF Model and Their Comparison to CASES-97 Observations. *Monthly Weather Review*, **141**, 30-54.
- Stull, R. B., 1988: An Introduction to Boundary Layer Meteorology. *Atmospheric Sciences Library*, **8**, 89.
- Talbot, C., E. Bou-Zeid, and J. Smith, 2012: Nested Mesoscale Large-Eddy Simulations with WRF: Performance in Real Test Cases. *Journal of Hydrometeorology*, **13**, 1421-1441.
- Wang, M., X. Xu, and H. Xu: The possible influence of the summertime deep atmospheric boundary layer process over the Taklimakan Desert on the regional weather. (*submitted to Quarterly Journal of the Royal Meteorological Society*).
- Xu, H., Y. Wang, and M. Wang, 2018: The Performance of a Scale-Aware Nonlocal PBL Scheme for the Subkilometer Simulation of a Deep CBL over the Taklimakan Desert. *Advances in Meteorology*, **2018**, 12.
- Zhang, F., Z. Pu, and C. Wang, 2017: Effects of Boundary Layer Vertical Mixing on the Evolution of Hurricanes over Land. *Monthly Weather Review*, **145**, 2343-2361.

1 **Performance of WRF Large-Eddy Simulations in summertime CBL**
2 **characteristics over the Taklimakan Desert: A Real Test Case**

3
4
5 Hongxiong Xu¹, Minzhong Wang¹²⁴, Yinjun Wang¹, Wenyue Cai¹³
6
7
8
9
10
11
12
13
14
15
16

17 1 State Key Laboratory of Severe Weather, Chinese Academy of Meteorological Sciences
18 Beijing, China 100081

19 2 Institute of Desert Meteorology, CMA (Chinese Meteorological Administration),
20 Urumqi, China

21 3National Climate Center, Chinese Meteorological Administration,
22 Beijing, China 100081

23 4 Taklimakan Desert Atmospheric Environment Observation Experimental Station, Tazhong 841000,
24 China

25
26
27
28
29
30 Submitted to *Journal of Meteorological Research*

31 January 2, 2018

32 Corresponding author:

33 Dr. Minzhong Wang

34 Institute of Desert Meteorology,

35 CMA (Chinese Meteorological Administration),

36 No. 46, Zhongguancun South Street, Haidian District, Beijing

37 P. R. China, 100081

38 Email: wangmz@idm.cn

39 dorn1984@163.com

40

41 **Abstract**

42 During the summer season over Taklimakan Desert, the maximum height of the CBL
43 (convective boundary layer) can exceed 5,000 m, which appeared to play critical roles in
44 simulating the regional circulation and weather. In this paper, we use a combination of WRF-LES
45 (Weather Research and Forecasting Model Large-Eddy Simulation), the GPS radiosonde and
46 eddy-covariance station to evaluate the performance of WRF-LES in the deep convective PBL
47 case over the central Taklimakan. Results show that the model reproduces reasonably well the
48 evolution of PBL processes. However, simulations are relative warmer and moister than those
49 observed due to the over-predicted surface fluxes and largescale advection. Tests are further
50 performed with multiple configurations and sensitive experiments. Sensitivity tests to Lateral
51 Boundary Condition(LBC) showed that the model results are very sensitive to changes in time
52 resolution and domain size of Specified LBC. It is found that larger domain size varies the
53 distance of the area of interest from the LBC, is efficient to reduce the influences of large forecast
54 error near the LBC. However, more frequently updated LBC is desirable to inhibit model error
55 near the LBC. On the other hand, model error increased as the distance between the area of
56 interest and the lateral boundaries decreased. Furthermore, comparing model results using the
57 original surface land parameterized sensible heat flux(SH) with Noah land-surface scheme and
58 those of sensitive experiment, it is concluded that the desert CBL is very sensitivity to SH
59 produced by surface land scheme during summer day time. A reduction in SH can correct
60 overestimate of the potential temperature profile. However, increasing SH significantly reduce the
61 total time needed for CBL increase to a relative low altitude (< 3 km) at the middle and
62 preliminary stage of the development of CBL rather than produce higher CBL at the late stage

63 Keyword: WRF, Large Eddy Simulation, Convective Boundary Layer, Taklimakan

64

65

For Review Only

66 1 Introduction

67 The Taklimakan Desert, locates at the south center of the province of Xinjiang, China, is
68 the world's second-largest flow desert and has profound influences on the regional weather
69 and climate. Because of the extreme near-surface temperatures, the Taklimakan PBL
70 (planetary boundary layer) commonly reaches 4–6 km during boreal summer(Wang et al.),
71 making it probably the deepest on earth. The deep PBL, which is significantly higher than that
72 of the surrounding mountains and oases, appeared to play important roles on regional
73 circulation and weather. In the northwest of china, the ability to accurately forecast in
74 Taklimakan Desert especially the PBL processes is an important problem.

75 The large desert (such as Sahara, Taklimakan et al.) atmosphere is always a key
76 component of the climate system. The surface heating from intense solar radiation leads to the
77 development of a near-surface thermal low pressure system, commonly referred to as the heat
78 low(Engelstaedter et al. 2015). However, despite of the vital role of the desert playing in the
79 climate system, observations are extremely sparse, and thin data that exist are mostly from the
80 surrounding of the desert due to the poor work and natural(Marsham et al. 2011). This
81 fundamentally restrict the development of understanding desert and surrounding area, and
82 leads to large discrepancies to analyses and significant biases in operational numerical
83 weather prediction (NWP) models, given the scarcity of observation being assimilated by
84 operational systems. The ability of these local models to simulate real-world cases is often
85 hindered by a lack of favorable data needed to assess the performance of model
86 results(Garcia-Carreras et al. 2015). To fill in the gaps of Taklimakan desert, the field
87 observation experiment was held during the month of July 2016 in Tazhong, which is located

88 at center of Taklimakan, by the Institute of Desert Meteorology (IDM), Chinese
89 Meteorological Administration (CMA), Urumqi(Liu et al. 2012; WANG et al. 2016a; Wang
90 et al. 2016b). This will also give the opportunity to evaluate the performance of the deep PBL
91 process in NWP models over Taklimakan.

92 On the other hand, atmospheric motions interweave small-scale, complex and multiscale
93 nonlinear interactions. Due to the limited resolution (time and space) mesoscale atmospheric
94 models are still **unable to** explicitly represent all these processes(Talbot et al. 2012). Such
95 processes include turbulent motions, which are too small-scale to be explicitly resolved in the
96 atmospheric model by a simplified process. Furthermore, turbulent mixing throughout the
97 PBL can heavily impacted NWP forecasting (Shin; Hong 2011; Shin; Hong 2015).

98 One way to tackle complex turbulent flows in weather forecast models is Large eddy
99 simulation (LES) which explicitly resolve energy-containing turbulent motions that are
100 responsible for most of the turbulent transport(Moeng et al. 2007). It has been used
101 intensively to examine detailed turbulence structure, to generate statistics, and to perform
102 physical-process studies(Garcia-Carreras et al. 2015; Heinold et al. 2013; Heinold et al. 2015;
103 Heinze et al. 2015; Sun; Xu 2009). However, most LES applications to the PBL have been
104 limited to idealized physical conditions. Recently, some studies attempt to test LES and assess
105 its performance in simulating real cases(Liu et al. 2011; Talbot et al. 2012). Liu et al. (2011)
106 suggests that WRF-LES is a valuable tool for simulating real world microscale weather flows
107 and for development of future real-time forecasting system, although further LES modeling
108 tests, such as elucidate whether inaccurate synoptic forcing or coarse resolution, are highly
109 recommended. Talbot et al. (2012) suggested that the ability of WRF-LES to simulate

110 real-world cases are hindered by a lack of favorable synoptic forcing. The initial(ICS) and
111 lateral boundary conditions(LBCS) was found to be more critical to the LES results than
112 subgrid-scale turbulence closures. Thus, the LBCS of can significantly alter high-resolution
113 LES status through inflow boundaries(Rai et al. 2017).

114 However, most of research above on LES over desert has been limited to idealized
115 physical conditions(Garcia-Carreras et al. 2015) or conducted real case outside
116 Taklimakan(Liu et al. 2011; Talbot et al. 2012). The aim of this study is the attempt to
117 applicate LES in a real deep CBL case over Taklimakan. An important aspect of the ongoing
118 this paper is to examine assess the skillfulness of WRF-LES in relative coarse resolution
119 (333m) over Taklimakan dessert in simulating real cases of deep desert PBL process during
120 boreal summer events in Taklimakan. First we use a combination of WRF-LES and the GPS
121 radiosonde and surface fluxes calculated by an eddy-covariance method taken in the central
122 Taklimakan to evaluate the performance of WRF-LES in real case. Then we assess the
123 potential errors related to LBC. Moreover, we aim to evaluate the relative contribution of
124 uncertainties in surface model to the typical behavior of PBL processes by conducting the
125 sensitivity experiments. Thus, the sensitivity of the performance to surface sensible heat flux
126 (SH) is also studied. Section 2 gives a brief description of synoptic of the study case, and we
127 described data and model configuration and design of numerical experiments used in this
128 study. We presented the results of numerical simulations in Section 4. Finally, we summarize
129 conclusions in Section 5.

130 2 Method

131 2.1 Model configuration

132 The WRF model of version 3.8.1 (Skamarock et al. 2008) is utilized here at
133 sub-kilometer resolutions to simulate the extreme CBL event in Taklimakan desert. The
134 model is integrated for 12h, starting from 0800 **BJT (Beijing Time)** 01 Jul 2016. We
135 conducted one-way nest WRF from mesoscale down to LES-scales. All domains were 51
136 levels extended to 50 hPa. **Height for lowest 20 levels are 1130.473, 1157.705, 1207.765,**
137 **1294.703, 1423.873, 1591.895, 1795.526, 2021.868, 2272.33, 2558.433, 2882.675, 3248.113,**
138 **3658.499, 4118.481, 4633.882, 5212.111, 5855.802, 6517.111, 7151.295, 7757.151.** The
139 model horizontal spacing is 12km 3km 1km and 0.33km for d01 d02 d03 and d04. The sizes
140 of model grids are 411 ×321 791x651 211x201 and 403x406 respectively. Figure 1 shows
141 the domain for all experiments **except for BDY_T3. Smaller grid sizes (205 X 208) are used**
142 **in experiment BDY_T3 to verify the effect of domain size on LES simulation.**

143 The initialized condition and lateral boundary conditions are provided to the coarsest
144 mesoscale simulations from NCEP Global Data Assimilation System (GDAS) Final
145 Operational Global Analyses. The analyses are 0.25-degree by 0.25-degree grids prepared
146 operationally every six hours and available on the surface, at 32 mandatory (and other
147 pressure) levels from 1000 millibars to 10 millibars (National Centers for Environmental
148 Prediction 2015).

149 The model physical options include the WSM5 microphysics scheme (Hong; Lim 2006),
150 the Yonsei University (YSU) planetary boundary layer scheme (Hong; Pan 1996), the Kain–
151 Fritsch cumulus parameterization scheme(Kain 1993; Kain 2004), **RUC (Rapid Update Cycle)**
152 **land-surface model**(Smirnova Tatiana et al. 2000; Smirnova et al. 1997), the Rapid Radiative
153 Transfer Model (Mlawer et al. 1997) longwave, and the Dudhia shortwave radiation scheme

154 (Dudhia 1989). The cumulus parameterization scheme is only applied to the d01(12km) grid
155 domain to parameterize the convective rainfall. While, the large-eddy-simulation (LES) is
156 only applied to d04(0.333km).

157 Table 1 shows the list of experiments. Experiment 1 was the control experiment, denoted
158 as CTRL. The experiment 2 (6-hour update LBC, denoted BDY_T2) and experiments 3(with
159 domain sizes 205 X 208, denoted BDY_T2) were conducted the same as CTRL with different
160 domain sizes and LBC update frequency. In experiment 4 (denoted HFX_%75) and 5
161 (denoted HFX_%125), the SH (sensible heat flux) was reduced to 75% and 125% of that in
162 the control experiment in the RUC land-surface scheme, to highlight the impact of SH on
163 deep CBL at Taklimakan desert, respectively. In experiment 6 (denoted Noah), Noah
164 land-surface model(Chen; Dudhia 2001a, 2001b) was used to replace the RUC land-surface
165 model in CTRL experiment to discriminate the influence of different land-surface model on
166 deep CBL.

167 2.2 Data

168 The model simulations are compared to the Tazhong field experiment, which was held
169 during the whole month of July 2016 in Tazhong, by the Institute of Desert Meteorology
170 (IDM), Chinese Meteorological Administration (CMA), Urumqi. The main station was
171 located at 86.63° E, 39.03° N. The location is relatively flat with few hills and covered by
172 sand combined with grass (Figure 1), and the deep PBL of our simulation was under a
173 cloudless sky and dry environment. Instruments are described as follows:

174 1) surface fluxes: The eddy correlation system was a R3-50 supersonic anemometer
175 developed by Gill Company, UK, deployed at a height of 10 m. The data acquisition

176 frequency was 20 Hz, and the surface sensible heat flux was calculated by the
177 eddy-covariance method.

178 2) vertical profiles measured using soundings: Upper air soundings of temperature,
179 pressure, humidity, and wind speed and direction were conducted 3-6 times per day with the
180 GPS sounding system developed by No. 23 Institute of China Aerospace Science & Industry
181 Corp. (CASIC23). The sounding times were 01:15, 07:15, 10:15, 13:15, 16:15 and 19:15
182 respectively.

183 2.3 Synoptic

184 Figure 2 shows the synoptic patterns at 0800 BJT 1 July 2016 at 850 700 500 and 100
185 hPa. There were cyclonic vortex from 850 to 500 hPa center at 55° N (Figure 2a ,b and c).
186 Taklimakan was located east of cyclonic vortex and embedded in east–west-elongated ridge
187 at 0800 BJT 1 July. To the southwest, influenced by the South Asia High, which was centered
188 over the eastern Iranian Plateau, the upper air over the Taklimakan Desert was controlled by
189 the westerly jet stream at 100hPa (Figure 2 d). The low-pressure system at low level, which
190 is termed of heat low (Figure 3), dominated most area of southern Xinjiang and resulted in
191 continuous high temperature over the desert. This situation favored the subsidence motion and
192 served as a triggering mechanism for deep PBL in the region in the coming 2–3 days (not
193 show).

194 3 Results

195 3.1 Validation of the deep CBL structure

196 Time series of surface variables at Tazhong station from CTRL simulation for 01 July
197 2016 are presented in Figure 4a, b. Results show that discrepancies of thermodynamic surface

198 variables (the surface temperature, sensible and latent fluxes) between model and observation
199 are large during simulation. The SH (surface sensible heat flux) is far less in observation
200 (maximum: 243 W m^{-2}) relative to model (maximum: 613 W m^{-2}). This represents SH from
201 WRF simulation is 2.5 times than that of observation when both of which reach its maximum.
202 On the other hand, model shows a significant cold bias for the surface temperature. The
203 surface temperature is much higher in observation (maximum: $70 \text{ }^\circ\text{C}$) relative to model
204 (maximum: $50 \text{ }^\circ\text{C}$). To further verification the surface variables, RMSE (root mean squared
205 error) and BIAS (mean bias) are calculated including integration hours from 3 to 12 h for
206 Tazhong station in Table 2. As mentioned earlier, model show yields significantly
207 overestimate of SH (RMSE 263.636 W/m^2 , BIAS: 250.14 W/m^2) and dramatically
208 underestimated of surface temperature (RMSE $14.65 \text{ }^\circ\text{C}$, BIAS: $-13.37 \text{ }^\circ\text{C}$).

209 Two possible reasons result in model SH far above that of observation: (1) The
210 mismatches of land-use between the model and the observation. WRF use land-use categories
211 to assign certain static parameters and initial values to each grid cell, for example, albedo,
212 surface roughness, and so on (Schicker et al. 2016). However, As in Figure 1c, the EC station
213 is surround by mixing land of grass and sand. The complex underlying surface may not be
214 adequately reproduced by model and can have an impact on the overestimate of SH in this
215 case. (2) It is should be noted that the SH and LH (latent heat flux) based on eddy
216 correlation might be underestimated (LeMone et al. 2013). Researchers found that if the other
217 two terms in the budget—net radiation and flux into the soil were accurate, used data for the
218 whole experiment to find the $H + LE$ for Tazhong station are equal to an average of 75% of
219 what would be required for balancing the surface energy budget.

220 **Despite the large differences on surface**, near-surface variables (2m temperature, relative
221 humidity and 10m wind speed, Figure 4 e f g) are closer to measurements than those from
222 surface, their values are relatively higher than those observed. The time series evolution of 2m
223 temperatures nearly follow those of the observations (**RMSE:1.66, BIAS:1.61**); but model
224 produce warmer surfaces by about 3 K at the beginning of model integration, and 1K when
225 model and observation both reach their maximum temperature, respectively.

226 Results indicate that, model-produced near-surface relative humidity is close to
227 observations at initial time (Figure 4 f). However, the humidity from the model keeps
228 increasing at the first few hours of model integration, when observations decrease. After 3
229 hours' spin-up, the model reproduces reasonably well the evolution of humidity, in agreement
230 with observation (**RMSE:1.22**), but their values are relative higher than those
231 observed(**BIAS:1.11**).

232 One reason for this discrepancy is the overestimate of soil moisture during simulation.
233 Soil moisture can severely impact near-surface humidity. The overestimate of the soil
234 moisture contents in the initial condition of the model, which are only offered to the model at
235 **initial time**, may result in considerable differences in near-surface layer humidity (Talbot et al.
236 2012). In the present simulations, model results are reported to produce grossly overestimate
237 soil moisture. At the model initialization for the CTRL simulation, EC station at Tazhong
238 station indicated a value of the 5-cm-deep soil moisture of $0.230 \text{ m}^3/\text{m}^3$, while the model
239 initial value is $0.6 \text{ m}^3/\text{m}^3$ (Figure 4 d). This large overestimate of soil moisture results in LH
240 (Figure 4 b, f) **from the model continue to increase. As a result, near-surface of model is far**
241 **moister than that of observation at the first few hours of model integration.** An interesting

242 result to note is that the model simulation has the abilities to correct some of the bias due to
243 the initial condition of the surface; The results from CTRL experiment are closer to
244 observation after 3 hours' spin-up.

245 The model simulated potential temperature are compared to GPS sounding
246 measurements at Tazhong during 0800~2000 BJT 01JULY2016 in Figure 5 (solid lines). **One**
247 **should note that radio-sounder floating about 7 Km away from Tazhong, when radio-sounder**
248 **reach 6 Km height. Thus, for comparison, the profiles of model simulations are averaged**
249 **station in a radius of 3.5 Km.** At 0800 BJT, when the model is initialized, the nocturnal
250 inversion reaches 300m (not shown). By 1100 BJT, this inversion is eroded in the model in
251 agreement with observations, and both reaching about 300m at 1100 BJT (Figure 5 a).
252 However, the simulated CBL grows faster in the morning due to larger SH than observation,
253 reaching 3500m (3000m in the observations) at 1400 BJT (Figure 5 b). At 1700 BJT (Figure 5
254 c), the simulated and observed CBL heights exceed 4000m and 5000m respectively. This
255 indicates that the simulated CBL grows more slowly in the afternoon than measurement.
256 Compared to measurements, the model is initially cooler with faster heating rate in the
257 morning. As a result, model is warmer than measurements in the afternoon. Eventually, model
258 agrees with observations at the end of the day. One possible minor reason is the differences of
259 potential temperature lapse rate above the top of mixing layer between observation and
260 simulation. Simulated stronger inversion layer restrain the development of CBL, which will
261 be discussed below.

262 Moreover, in terms of CBL temperatures, the model initially simulates a cooler and drier
263 CBL than that observed, at 1100 BJT01 JUL (Figure 5a). Compared to the observed potential

264 temperature profile, the CBL seems to appear earlier in model forecasts result based on
265 obvious warming in surface layer. One should note that RL (residual layer) may play a key
266 role in the deep PBL at Taklimakan desert. At 1100 BJT, when the CBLH was about 300 m in
267 observation as show above, potential temperature in the were about 317 in PBL and 320 K in
268 RL, respectively. When the potential temperature in CBL increased to the value in RL (320
269 K), the CBL merged with the RL, and the height of PBL reach 3000m in the observations at
270 1400 BJT. These results are in good agreement with Han et al. (2012). By analysis of
271 observation of a CBL in the Badanjilin region, they found a rapid development process of
272 CBL after 1200 LST, which appeared to be a jump of CBLH when the inversion layer
273 vanished.

274 When the SH reaches its maximum at 1400 BJT (Figure 5b), potential temperature
275 profile is closer to measurements than at initial time, and their values are higher than those
276 observed. By 2000 BJT (Figure 5d), CBLH in the model reaches its maximum value, which is
277 consistent with observation, despite of approximately 0.4K cooler on the lower
278 levels(<2.5Km). As mentioned, one cause of the higher temperatures produced with
279 model would be the large difference in the surface heat fluxes. It was concluded that
280 the surface sensible heat flux from the land surface parameterization is the crucial
281 factor affecting the CBL process during summer day time. Differences in surface SH
282 would create differences in the vertical development of the PBL. Thus, the large
283 surface SH difference between the model and observation may lead to differences in
284 CBL growth during daytime and in its peak depth during the simulation. Fortunately,
285 one can artificially modify the surface SH computed by surface-land model, which

286 controls the calculation of surface fluxes. Sensitive simulations will be realized and
287 discussed **in next section**.

288 Figure 5 also shows Vertical profiles of vapor mixing ratio (**dash lines**) at Tazhong
289 station. The simulated profiles with lower RL are much drier than observation from 1500 to
290 3500m at 1100 BJT. The vertical mixing results in the uniform structure of vapor mixing ratio
291 within CBL, so the differences between simulated and observational profiles are reduced
292 remarkably when CBL reach above 4000m at 1400 BJT. Differences are generally less than
293 1g/Kg at 1100 BJT reaching a maximum of 0.3g/Kg at 1400 BJT. However, measured PBL
294 moisture shows an inverse layer at lower PBL($\leq 2000\text{m}$) range from 2.8 to 3.6 g/Kg, which is
295 not captured by model. Furthermore, as the convective boundary layer grows, the inversion
296 moisture structure below 3000m develops to and maintains below 3000m during 1400~2000
297 BJT. By the end of the day, the model-simulated CBL humidity show moister than
298 observation, **because model cannot reproduce the inverse moisture layer within CBL**.

299 Inverse humidity may be caused by the joint of the heterogeneous humidity Pattern and
300 Large-scale advection over the underlying surface. For instance, interaction of oasis with
301 desert environment may resulted in the inverse humidity layer in desert PBL. Thus, one
302 possible reason for the discrepancy between model and observation caused by the error in
303 land-use type. The USGS land-use in ARW-WRF is based on AVHRR (Advanced Very High
304 Resolution Radiometer) 1km resolution satellite data during 1992-1993. For our case, this
305 land-use data may be outdated in Taklimakan. Besides such changes, misclassifications are
306 found in the USGS land-use data, the default land-use dataset in WRF(Schicker et al. 2016).
307 This is also confirmed by the discrepancies of land-use between simulation and measured at

308 the Tazhong station in the previous figure. Large-scale advection of dry air can affect the
309 profile of moisture. Moisture will also be variable in the horizontal, so advection at the low
310 level could contribute to the dry at bottom and moisture at the upper of PBL between 1100
311 and 2000 BJT at the bottom of the PBL.

312 The mismatch between the model and the observations in terms of moisture that is
313 present means that the effect of land-use type and Large-scale advection needs to be
314 quantified and that more detailed data of Taklimakan (land and atmosphere) might be
315 necessary to realize a more realistic performance. Extra care should also be taken with sparse
316 and the limited data in the periphery of the Taklimakan (ter Maat et al. 2012).

317 **3.2 Sensitive to Lateral Boundary Condition(LBC)**

318 **After verifying** the details of the LES simulations, we assess the sensitivity of the LES
319 simulations to time resolution and domain size of Specified LBC. For one-way nest, Specified
320 LBC **is** obtained from coarser model simulation. The analysis and all forecast times from a
321 previously-run larger-area model simulation are used to specify the LBC. The primary cause
322 of differences in PBL structure was diagnosed as differences in domain size and frequency
323 provided by the coarser resolution. The aim is to assess the sensitivity of the finer large-eddy
324 simulations to time frequency and domain size of Specified LBC forcing by larger-area model
325 simulation; Details of the three simulations (CTRL, BDY_T2 and BDY_T3) are given in
326 section 2.

327 Figure 5 compare the profiles of the simulated potential temperature and vapor mixing
328 ratio profiles from LBC sensitivity experiments and observation. Results indicate that, there is
329 a distinct relationship between LBC and CBL development. All model-produced profiles are

330 nearly the same at initial time (not show). However, the comparison results reveal that
331 discrepancies among different experiments are large for CBL. The results indicate that larger
332 domain size and more time frequency LBC leads to a warmer and drier PBL, but a cooler and
333 moister free troposphere. Such sensitivity is monotonic with respect to LBC (Figure 5).
334 Furthermore, in the next three hours, the differences between the sensitive experiments keep
335 increasing with time (Figure 5 a, b). The potential temperature profiles within CBL become
336 divergence at 1100 BJT. However, the results show more convergence at afternoon as CBL
337 continues to grow (Figure 5 c). Finally, largest discrepancies are found by end of the day
338 (Figure 5 d) where the model CBL potential temperature is warmer by up to about 0.7K and
339 0.9K in BDY_T2 and BDY_T1 respectively, compared to measurements.

340 Figure 6 shows cross sections along 39.03°N of horizontal winds, superposed with theta
341 and vapor mixing ratio. Overall, the **lower** frequently updated LBC is desirable to cold zone
342 near the LBC, which results in cold advection of the temperature and moisture to the area of
343 interest (Figure 6 b, c). Larger domain size, which varies the distance of the area of interest
344 from the LBC, is efficient to reduce the influences of large forecast error near the LBC to the
345 area of interest (CMP Figure 6 a, c). The results suggest that the model results are sensitive
346 to changes in time resolution and domain size of Specified LBC. The mismatch among
347 sensitive experiments is present means that the effect of LBC needs to be quantified to realize
348 a more realistic performance in the sub-kilometer simulations.

349 **To further examine the impact of LBCS on the turbulence of deep Taklimakan desert**
350 **CBL, the instantaneous vertical velocity fields for the horizontal are displayed in . By 1400**
351 **BJT, the convection of CTRL simulation obviously intensified under strong surface heating**

352 (Xu et al. 2018). Thus, the maximum vertical velocity reaches 9 m/s and the depth of mixed
353 layer grows to about 4.3 km (a). The distances between the boundary layer rolls
354 correspondingly increase to about 12 km and the height of the peak updraughts is raised to
355 just under 4 km. The cellular shape of updraughts and downdraughts characteristic of
356 boundary layer rolls is obvious in the horizontal view with the strength of convection.
357 BDY_T2 and BDY_T3 experiments (b, c) both reproduce motions with much weaker
358 maximum and minimum values at boundary of domain. In BDY_T3 experiment, Tazhong
359 station at center of the model has been directly influenced by the inflow cold advection
360 produced by low frequency LBCS and results in much weaker maximum and minimum value
361 of w (about 6 m/s). However, despite the underestimate of potential temperature, the w fields
362 for BDY_T2 experiment look similar to the CTRL w in plain view, and the horizontal extent
363 of the updrafts/downdrafts agrees with the CTRL as can be inferred from . To further examine
364 vertical structure of desert CBL, vertical cross-sections along Tazhong station (39°N) of w
365 are presented in Figure 8. Wide and regularly spaced updrafts along A1- A2 split into the
366 stronger and more irregular motions in CTRL and BDY_T2. The updrafts are much weaker in
367 the BDY_T3 experiment, as can be seen from Figure 8 c. Peak updrafts on BDY_T3 are about
368 4 m/s much weaker than on CTRL (9 m/s) and BDY_T2 (8 m/s). For BDY_T2 and BDY_T3,
369 the distant of the inflow boundary is wider, and the intensity of the convection is weaker at
370 the boundary. Compared with BDY_T2, the horizontal distribution of vertical velocity at
371 Tazhong station in BDY_T3 experiments is much weaker.

372 3.3 Simulations with different surface sensible heat flux (SH) and surface-land 373 models

374 The import cause of differences in PBL structure was diagnosed above as differences in
375 SH predicted by the surface-land schemes. The SH is one of the key factor affecting the
376 CBLH during summer day time. Thus, the difference between model and observation may
377 lead to differences in PBL growth during daytime; To further confirm whether this indeed
378 occurs, **three** additional sensitive simulations were realized based on the CTRL experiment.
379 **For Noah experiment Noah land-surface model is used to replace RUC land-surface model in**
380 **CTRL experiment, and for HFX-125%, HFX -75% SH is %125 and %75 that of CTRL (HFX**
381 **-100%)** experiment, while the other parameters remain the same.

382 The results **from Figure 10** and Table 2 showed that HFX-75% successively improved
383 the simulation of SH with RMSE:151.12, compared that of 263.64, 357.11 in CTRL and
384 HFX-125%. Of interesting is that experiment with Noah surface-land yielded the best
385 performance among all of the cases in SH, surface temperature and air temperature. However,
386 Noah surface-land model show large discrepancies with observation in Soil moisture, and
387 results in dramatically overestimate of LH and relative humidity compared to CTRL.

388 Further examining potential temperature and vapor mixing ratio (**Figure 9**) indicate that
389 with smaller SH leads to a cooler, moister lower PBL and a warmer, drier free atmosphere.
390 Such sensitivity is monotonic with respect to SH. Overall, the CBL structure from the
391 **HFX-75% and Noah experiments match** the GPS measurements better than the CTRL
392 (HFX-100%) simulations. Potential temperature profiles from CTRL (HFX-100%) and
393 HFX-125% are consistently warmer than the observation by about 0.4 and 0.5 K respectively,
394 while results from **HFX-75% and Noah** are within about 0.2K at 1400 BJT (**Figure 9** b). The
395 results suggest that the model results are sensitive to changes SH from land-surface model.

396 However, simulations converge at the end of the day, but remain differences at 2000 BJT
 397 (Figure 9 d). HFX-75% and Noah with weaker surface sensible heat flux can still produce the
 398 deep CBL nearly the same as CTRL and HFX-125%. This indicates that SH may not the
 399 dominant factor for the deep CBL over the Taklimakan desert.

400 Results of simulations on desert PBL in the morning agree with the previous studies of
 401 sensitivities land-surface model for other areas (Hu et al. 2010; Zhang et al. 2017). However,
 402 during 1700~2000 BJT 01July (Figure 9b, d), all experiments produce nearly the same CBLH
 403 and moisture in agreement with observation in the PBL. The effects of SH on the evolution of
 404 Taklimakan PBL structures during this period are needed to be further examined and
 405 discussed. So, the question is: why are simulations insensitive to land-surface process by the
 406 end of the day? As in Stull (1988), the development of CBL is mainly influenced by the effect
 407 of thermodynamic and turbulent entrainment without considering large scale factors such as
 408 large scale advection or subsidence. Besides the surface sensible heat, the intensity of
 409 entrainment process determines the increasing rate of CBL. Thus, the entrainment rate w_e is a
 410 valuable indicator for the development of PBL structure.

411 The rate of growth of the convective boundary layer is mainly determined by the
 412 entrainment rate w_e at the inversion layer without considering large scale vertical motion. w_e
 413 usually has a positive correlation with heat flux amount at the inversion layer $\overline{(w'\theta'_v)'}_h$, and
 414 large LES experiments show $\overline{(w'\theta'_v)'}_h$ is about 0.2 times the surface flux of buoyancy
 415 $\overline{(w'\theta'_0)'}$. During the period from 1100 to 1400 BJT, larger SH is obviously correlated with
 416 stronger turbulent entrainment and warmer air from free atmosphere (FA) entraining into ML.
 417 As a result, CBL develop rapidly and is warm too fast in the early simulation phase due to the

418 obviously increasing temperature and strong vertical mixing in model. Of interesting is that
419 reduction in SH reproduces better desert PBL evolution in the early simulation phase, as
420 SH-75% and Noah produce the smallest simulation errors in both temperature and moisture.
421 However, one should note that CBLH and potential temperature for SH-75% and Noah have
422 reached above 5000 m and 323.2 K respectively at 1700 BJT (Figure 9 a). For the rest of the
423 day, the increase rate of CBL height slows down due to the deep CBL(>5000m) which require
424 more heat for the growth of PBL depth; Moreover, w_e decrease with increasing inversion
425 intensity, which inhibits the mixing and entrainment processes. These two factors obviously
426 limit the growth of CBL when CBLH is over 5000 m in this deep desert CBL case. Therefore,
427 increasing SH from 75% to 125% significantly reduce the total time needed for CBL increase
428 to a relative low altitude (< 5 km) at the middle and preliminary stage of the development of
429 CBL rather than produce higher CBL at the late stage. When height of CBL over Taklimakan
430 desert exceeds 5000 m, it might not change with proportion to SH fluxes (Figure 9 d). As a
431 result, PBL of WRF simulations are basically the same, and not sensitive to SH fluxes by the
432 end of the day.

433 **4 Summary**

434 This paper assesses the performance of the Weather Research and Forecasting Model
435 (WRF) Large-Eddy Simulations(LES) in deep convective PBL case over Taklimakan Desert.
436 Tests are performed with multiple configurations and sensitive experiments. Sensitivity tests
437 to Lateral Boundary Condition(LBC) showed that the model results are sensitive to changes
438 in time resolution and domain size of Specified LBC. It is found that larger domain size varies
439 the distance of the area of interest from the LBC, is efficient to reduce the influences of large

440 forecast error near the LBC.

441 Consequently, with the configuration used in this study, the model reproduces
442 reasonably well the evolution of PBL processes. The model shows discrepancies between the
443 main CBL characteristics in the morning including the thermal and moisture structure. The
444 model simulates the relatively colder and drier morning CBL well, underestimating it by up to
445 1.5K near-surface layer at Tazhong station. In the case of the underestimation of moisture by
446 only up to 1 g/kg in the near-surface layer. The overestimation of CBL profile may be caused
447 by discrepancy between model and measurement initially. This indicates that the results are
448 sensitive to the model initial conditions. An interesting result to note is that the model
449 simulation seems to be able to correct some of the bias due to the initial condition. In the
450 afternoon, the model correctly reproduce the thermal structure, but simulations are relative
451 warmer and moister than those observed. Potential temperature profile at CBL appears
452 warmer by up to about 0.4K compared to the observations. While the model overestimates the
453 afternoon moisture seriously, it mainly overestimates vapor mixing ratio by about 1 to 2 g/Kg
454 in the CBL. Largest discrepancies are found in 0~3Km where the model vapor is twice as
455 moist (up to about 3g/Kg above AGL) as observed.

456 Furthermore, three additional sensitive simulations were realized to further confirm
457 whether large differences of SH lead to differences in ABL growth during daytime, based on
458 the CTRL experiment. The results suggest that the model results are sensitive to changes
459 SH and different land-surface models. The large difference between the model and
460 observation may lead to differences in CBL growth during daytime. From these results, it was
461 concluded the surface sensible heat flux is an important factor affecting the CBL depth over

462 Taklimakan during summer day time. However, its peak depth during the simulation show
463 less sensitive to SH because of decreasing w_e by the end of the day.

464 The future work aimed to study several other deep CBL cases over Taklimakan to
465 summarize their common features. Furthermore, we hope to utilize high resolution model and
466 observation to describe the fine characteristics of a typical deep Taklimakan CBL particularly
467 the turbulent and vertical mixing and its impact on regional weather forecast. This research is
468 aimed to improve the understanding of deep CBL over Taklimakan and its influence on
469 regional weather and climate.

470 **Conflict of Interests**

471 The author declares that there is no conflict of interests regarding the publication of this paper.

472 **Acknowledgments**

473 This study is supported by the National Natural Science Foundation of China (Grant no.
474 41575008 and 41775030). The author would like to thank all the reviewers and editors for
475 their professional advice to improve the paper.

476

477 Captions:

478 Figure 1 Simulation domains used in ARW model with terrain height (shaded, units:m); (b) land
479 use categories for domain D03 and D04.

480 Figure 2 Horizontal distribution of geopotential height (solid, units: dagpm), wind speed (shaded,
481 units: knot), and wind barbs from the NCEP FNL analysis at 0800 BJT 1 Jul 2016 at (a)
482 850 hPa, (c) 700 hPa, (e) 500 hPa, and (d) 100hPa.

483 Figure 3 NCEP FNL 700hPa potential temperature (colors) and mean sea level pressure (white
484 lines) at 0800 BJT 1 Jul 2016. The black dot shows the location of Tazhong station at
485 Xingjiang province.

486 Figure 4 Time series of simulated surface variables **from innermost domain of simulations**
487 **and surface observations at Tazhong station** (83.63° E, 39.03° N) initial at 0800
488 BJT 01July 2016 (a) sensible heat flux (W/m^2), (b) latent heat flux(W/m^2), (c) 2-m
489 temperature ($^{\circ}C$), (d) surface temperature ($^{\circ}C$), (e) 2-m Relative Humidity(%) and (f)
490 10-m wind speed (m/s) with corresponding observations.

491 Figure 5 Vertical profiles of potential temperature (solid line, units: K) and vapor mixing
492 ratio(dash line, units: g/Kg)from innermost domain **of simulations and observation of**
493 **GPS sounding at Tazhong station** (83.63° E, 39.03° N) at (a)1100 (b) 1400 (c)
494 1700 (d) 2000 BJT 01 Jul2016.

495 Figure 6 cross sections along $39.03^{\circ}N$ of horizontal winds (barbs, units: m/s), at intervals of 5 m/s,
496 superposed with theta (shaded, units: K) and vapor mixing ratio(contour, units: g/Kg), from (a)
497 BDY_T1, (c) BDY_T2, (e) BDY_T3 experiments at1400 BJT 01JUL2016, (b), (d), (f) are the
498 same as (a), (c), (e), but for 2000 BJT 01JUL2016.

499 Figure 7 Instantaneous vertical velocity fields (shading: m/s) at 3000 m for (a) BDY_T1 (CTRL), (b)
500 BDY_T2, (c) BDY_T3, and (d) Noah at 1400 BJT, 1 July 2016.

501 Figure 8 Vertical cross-section of instantaneous vertical velocity fields (shading: m/s) along
502 A1-A2 in for for (a) BDY_T1 (CTRL), (b) BDY_T2, (c) BDY_T3, and (d) Noah at 1400 BJT,
503 1 July 2016.

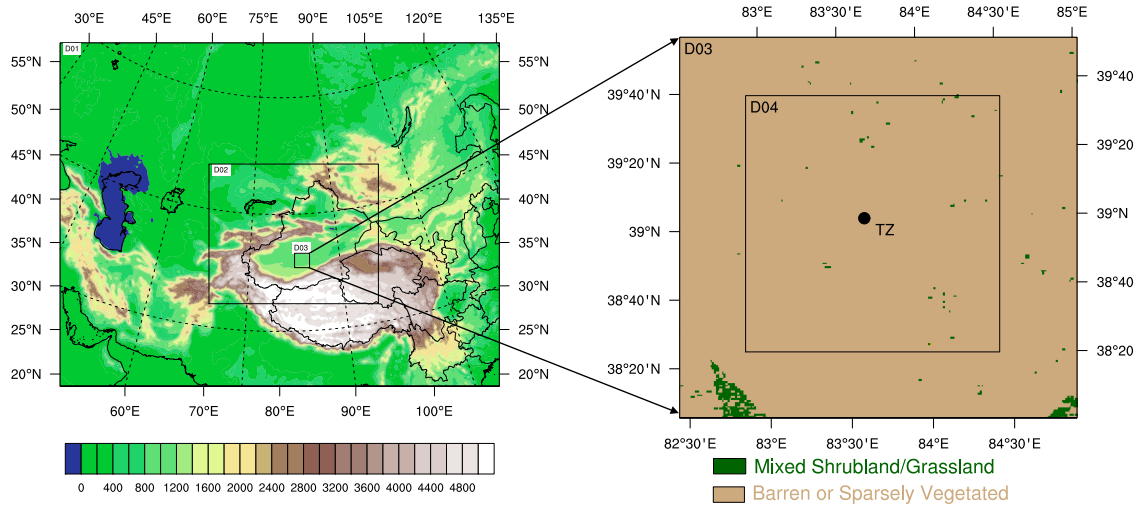
504 Figure 9 The same as Figure 5, but for SH flux sensitive and Noah land-surface experiment.

505 Figure 10 The same as Figure 4, but for SH flux sensitive and Noah land-surface experiment.

506

507

For Review Only



508

509

(a)

(b)



(c)

510

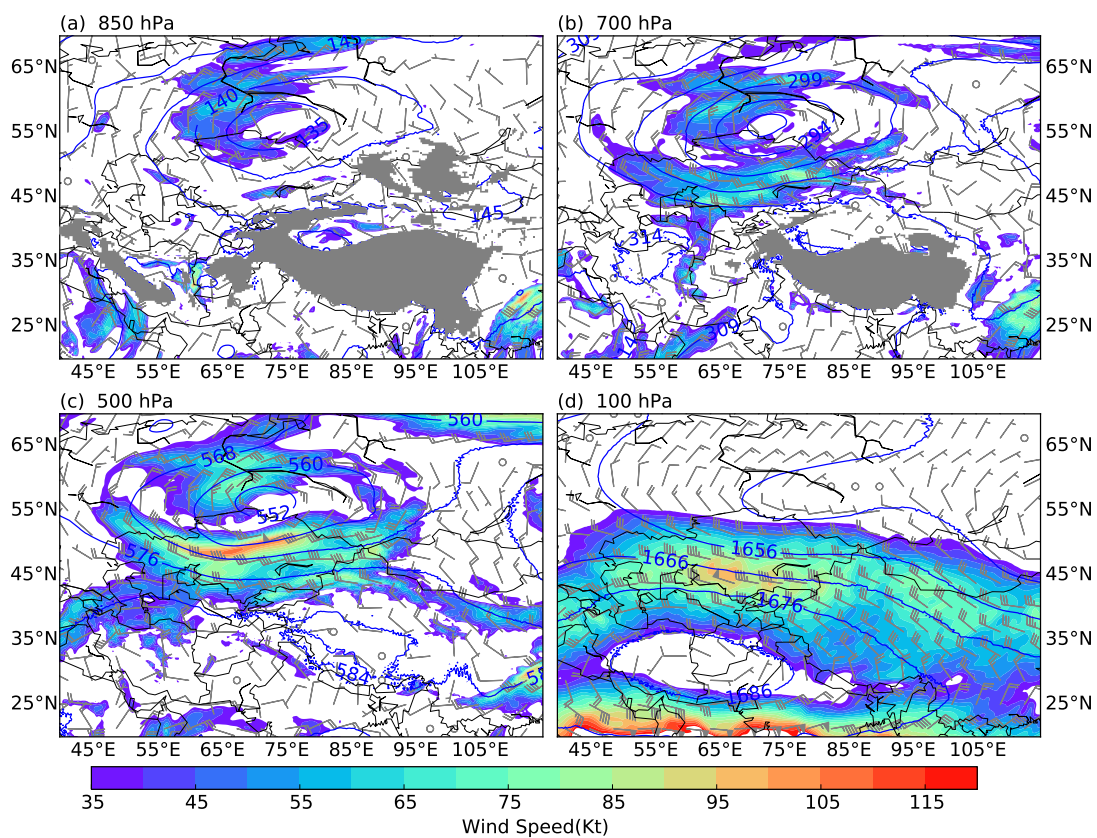
511

512 Figure 1 Simulation domains used in ARW model with terrain height (shaded, units:m); (b)

513 land use categories for domain D03 and D04; (c) photograph of Tazhong station

514

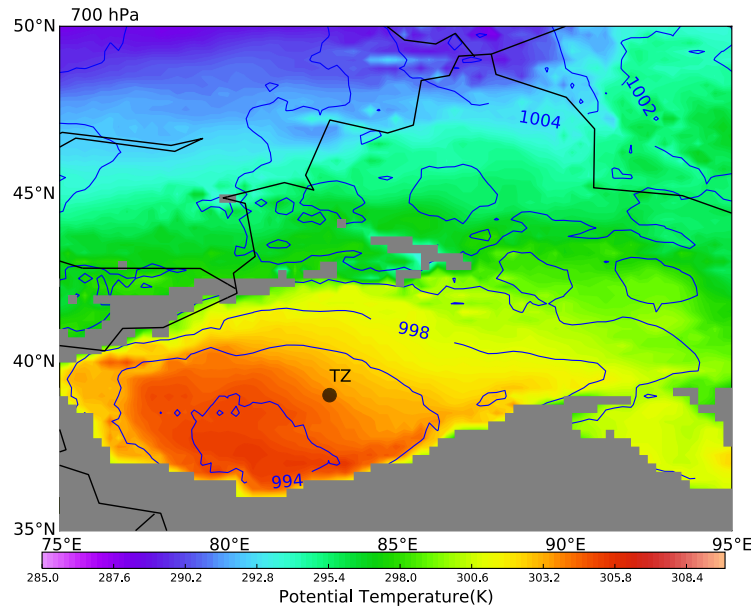
515



516

517 Figure 2 Horizontal distribution of geopotential height (solid, units: dagpm), wind speed
 518 (shaded, units: knot), and wind barbs from the NCEP FNL analysis at 0800 BJT 1 Jul 2016 at
 519 (a) 850 hPa, (c) 700 hPa, (e) 500 hPa, and (d) 100hPa.

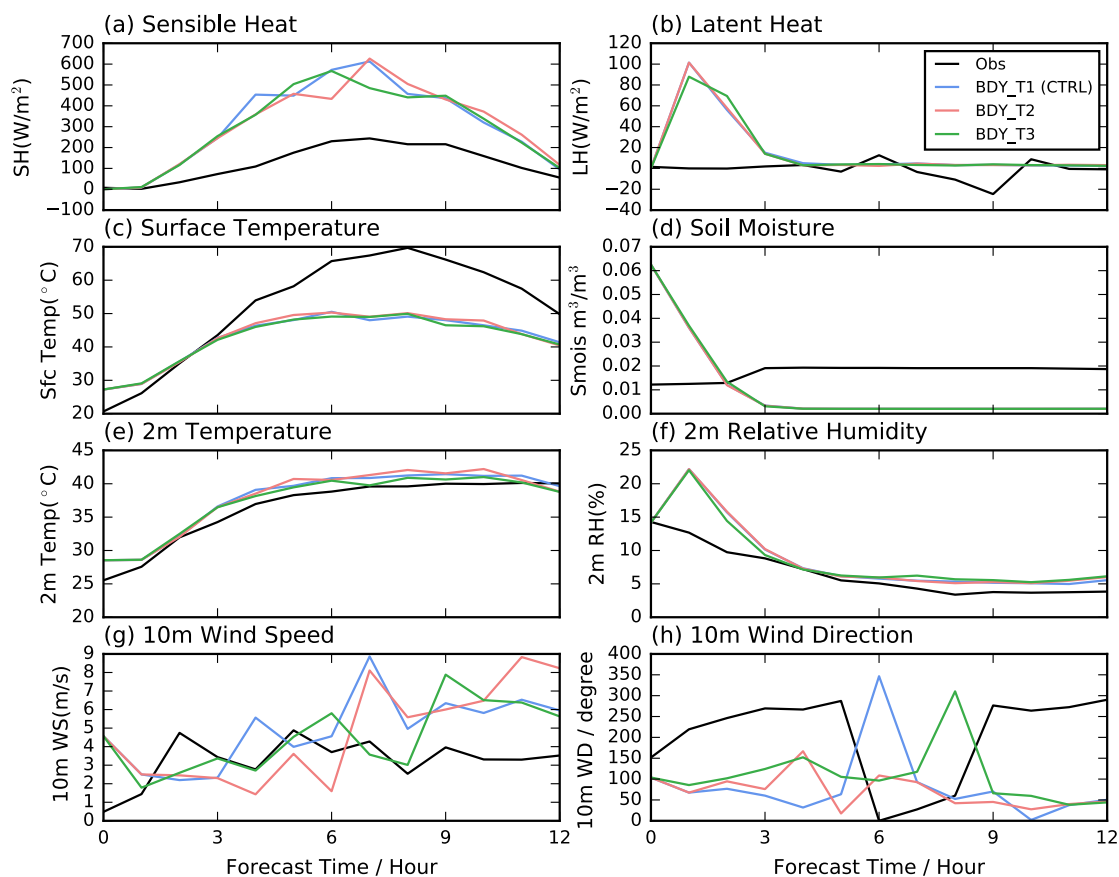
520



521

522 Figure 3 NCEP FNL 700hPa potential temperature (colors) and mean sea level pressure (white lines) at

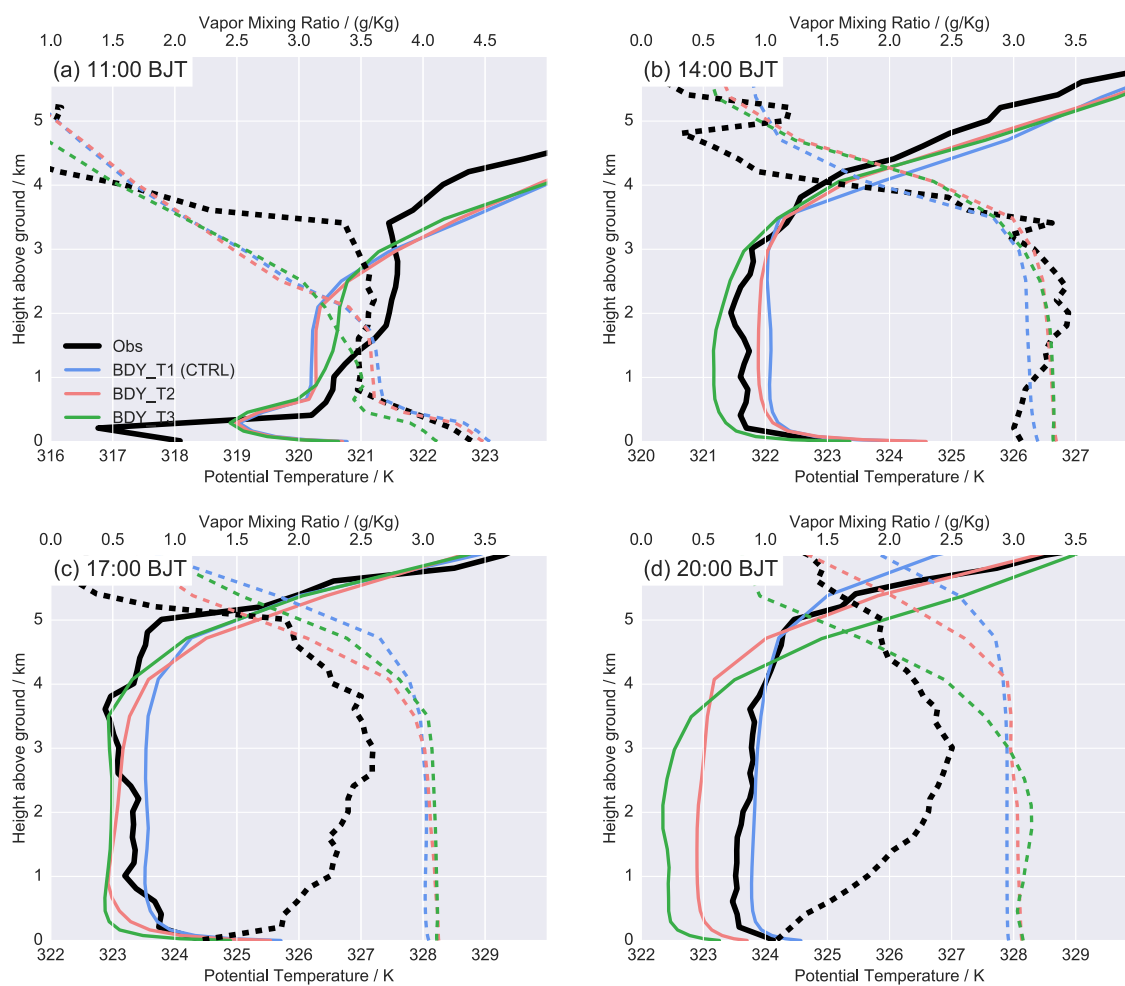
523 0800 BJT 1 Jul 2016. The black dot shows the location of Tazhong station at Xingjiang province.



524

525 Figure 4 Time series of simulated surface variables from innermost domain of simulations
 526 and surface observations at Tazhong station (83.63° E, 39.03° N) initial at 0800 BJT 01July
 527 2016 (a) sensible heat flux (W/m^2), (b) latent heat flux(W/m^2), (c) 2-m temperature ($^{\circ}\text{C}$), (d)
 528 surface temperature ($^{\circ}\text{C}$), (e) 2-m Relative Humidity(%) and (f) 10-m wind speed (m/s) with
 529 corresponding observations.

530



531

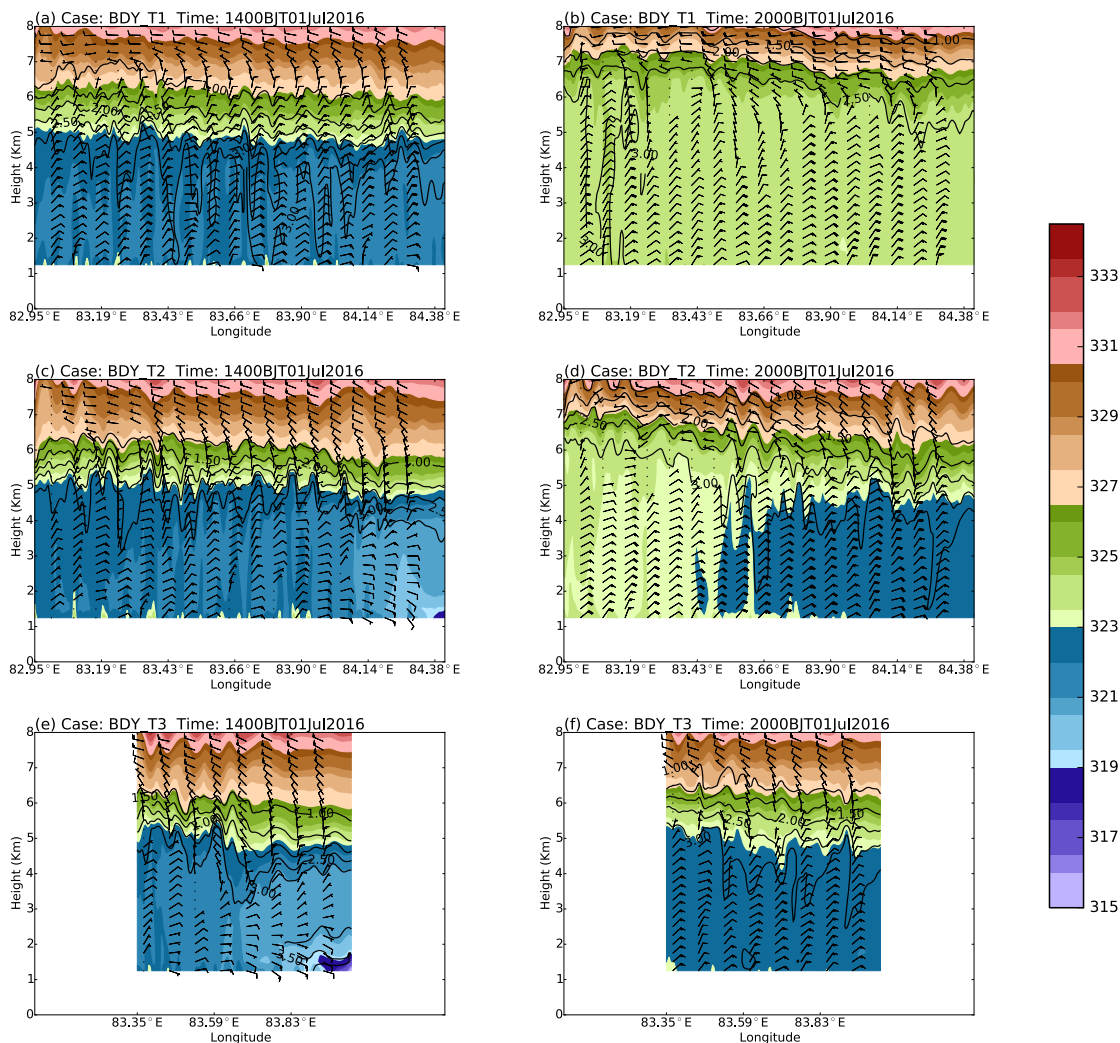
532 Figure 5 Vertical profiles of potential temperature (solid line, units: K) and vapor mixing

533 ratio(dash line, units: g/Kg)from innermost domain of simulations and observation of GPS

534 sounding at Tazhong station (83.63° E, 39.03° N) at (a)1100 (b) 1400 (c) 1700 (d) 2000 BJT

535 01 Jul2016. The profile of model output are averaged in a radius of 3.5km.

536



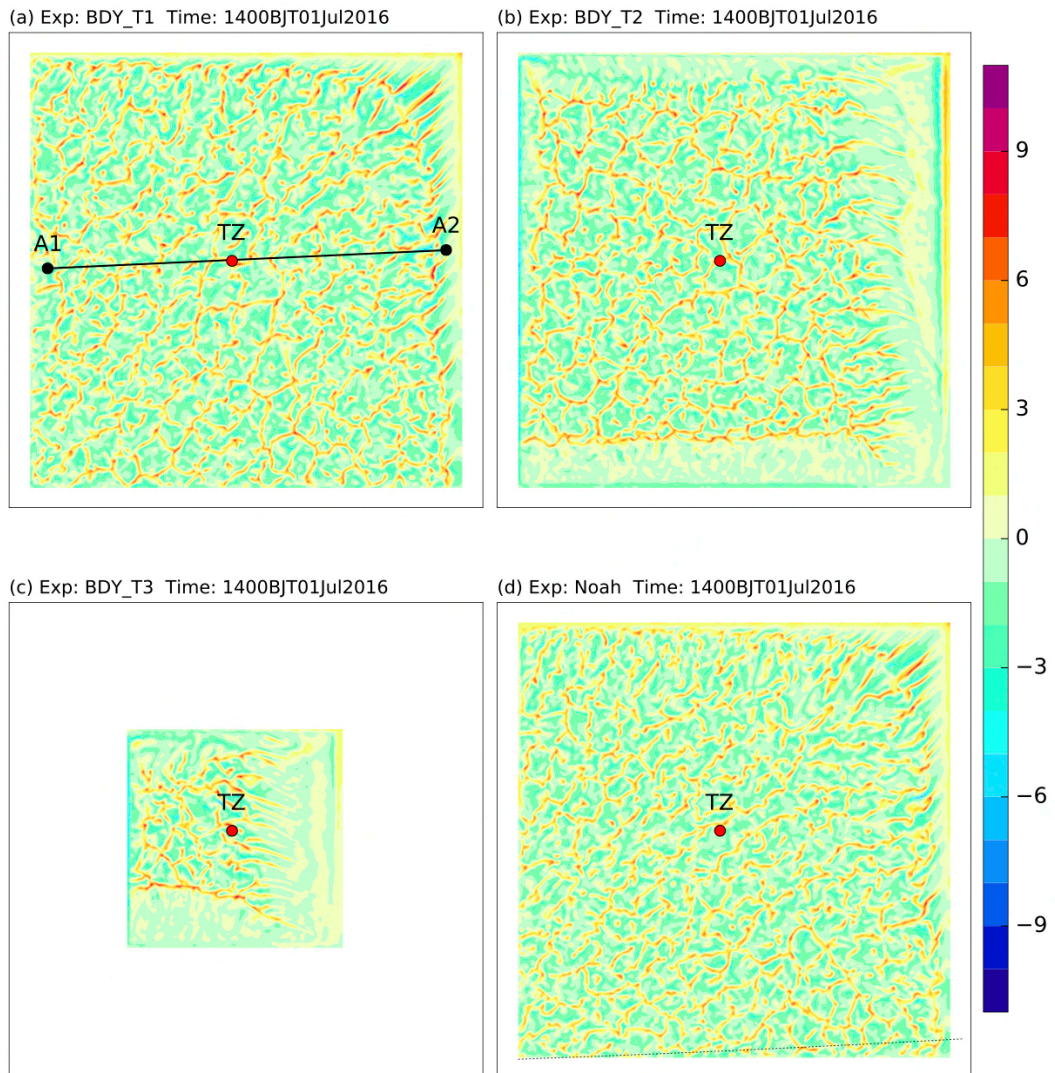
537

538 Figure 6 cross sections along 39.03°N of horizontal winds (barbs, units: m/s), at intervals of 5
 539 m/s, superposed with theta (shaded, units: K) and vapor mixing ratio(contour, units: g/Kg),
 540 from (a) BDY_T1, (c) BDY_T2, (e) BDY_T3 experiments at 1400 BJT 01JUL2016, (b), (d),
 541 (f) are the same as (a), (c), (e), but for 2000 BJT 01JUL2016.

542

543

544

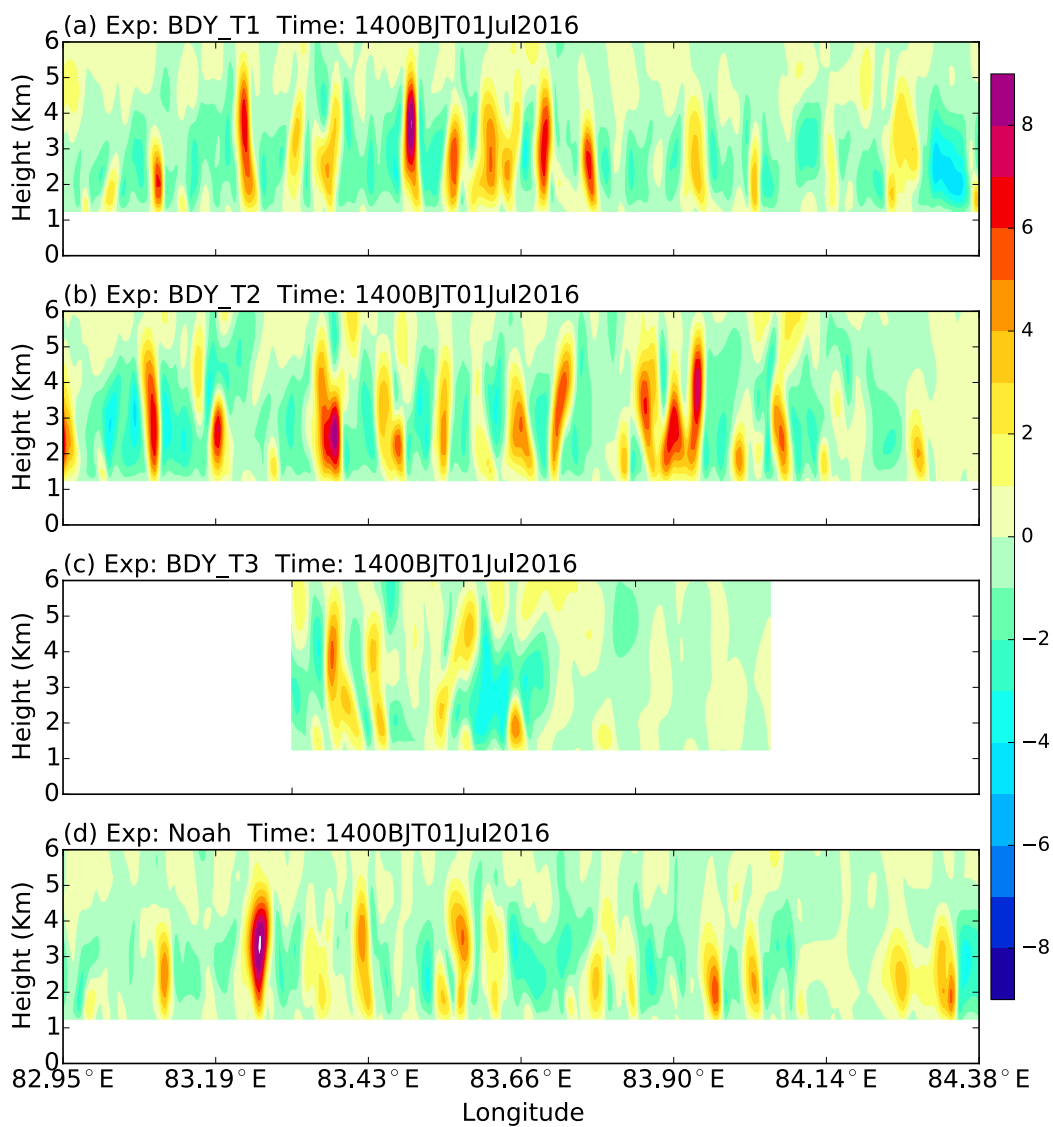


545

546 Figure 7 Instantaneous vertical velocity fields (shading: m/s) at 3000 m for (a) BDY_T1 (CTRL), (b)

547 BDY_T2, (c) BDY_T3, and (d) Noah at 1400 BJT, 1 July 2016.

548



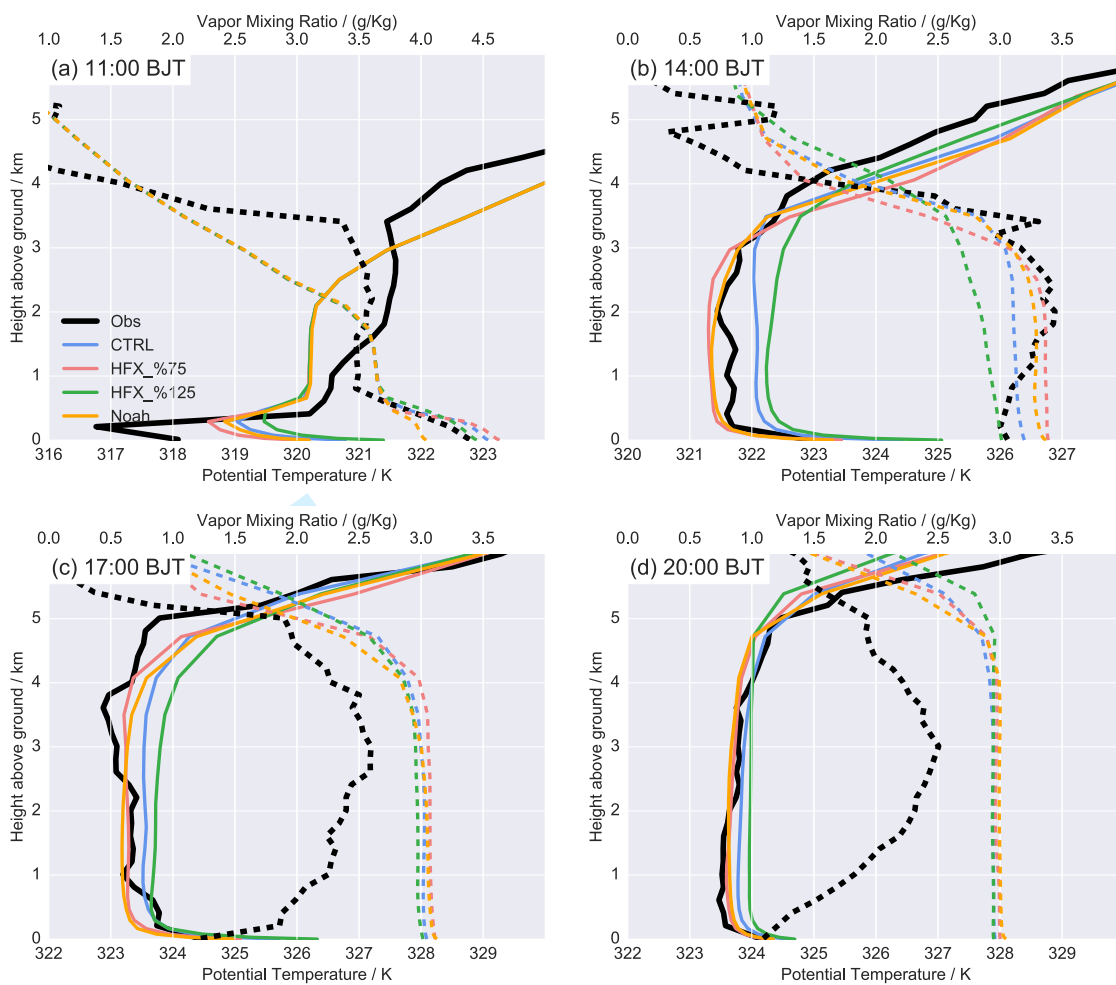
549

550 Figure 8 Vertical cross-section of instantaneous vertical velocity fields (shading: m/s) along
 551 A1-A2 in for for (a) BDY_T1 (CTRL), (b) BDY_T2, (c) BDY_T3, and (d) Noah at 1400 BJT, 1 July
 552 2016.

553

554

555

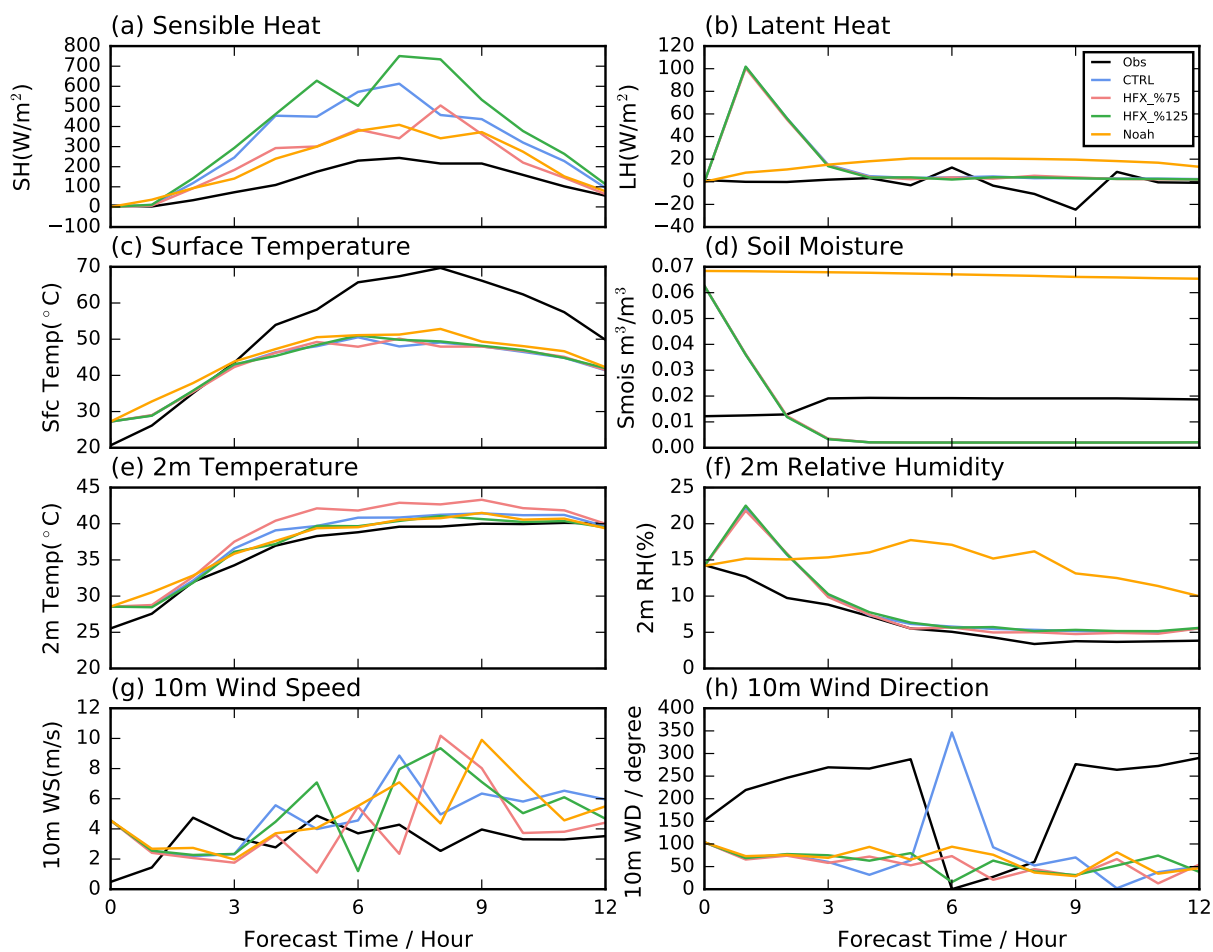


556

557

558

Figure 9 The same as Figure 5, but for SH flux sensitive and Noah land-surface experiment



559

560 Figure 10 The same as Figure 4, but for SH flux sensitive and Noah land-surface experiment.

561

562

Experiment	Name	Remarks
1	BDY_T1(CTRL)	LBC of D04 is provide by d03 every 1 hour with model grids 403x406
2	BDY_T2	As BDY_T1, but LBC of D04 is provide by d03 every 6 hour
3	BDY_T3	As BDY_T2, but with model grids 205 x 208.
4	HFX_%75	As CTRL_T2, but with SH 75%.
5	HFX_%125	As CTRL_T2, but with SH 125% .
6	Noah	As CTRL_T2, but with Noah surface-land model.

563

Table 1. List of designed experiments.

564

565

Variables	Sensible Heat		Latent Heat		Surface Temperature		Soil Moisture		2m Temperature		2m Relative Humidity		10m Wind Speed	
	RMSE	BIAS	RMSE	BIAS	RMSE	BIAS	RMSE	BIAS	RMSE	BIAS	RMSE	BIAS	RMSE	BIAS
Experiments														
CTRL	263.636	250.140	12.398	6.674	14.654	-13.373	0.017	-0.017	1.666	1.613	1.220	1.109	2.579	1.864
BDY_T2	249.395	240.660	12.383	6.253	14.116	-12.853	0.017	-0.017	1.912	1.817	1.275	1.162	2.943	1.307
BDY_T3	241.681	232.705	12.251	6.328	14.929	-13.737	0.017	-0.017	1.227	1.046	1.483	1.280	2.118	1.287
HFX_%75	151.119	134.594	12.544	6.354	14.740	-13.426	0.017	-0.017	3.078	3.016	0.956	0.826	3.335	0.874
HFX_%125	357.711	335.556	12.439	6.152	14.244	-13.043	0.017	-0.017	1.026	0.860	1.303	1.231	3.265	2.052
Noah	125.695	120.313	23.350	20.664	12.757	-11.502	0.048	0.048	1.046	0.983	10.116	9.904	2.788	1.795

566

567 Table 2. Summary of surface and air variables verification including integration hours from 3 to 12 h for Tazhong station.

568

569 **Reference:**

- 570 Chen, F., and J. Dudhia, 2001a: Coupling an Advanced Land Surface–Hydrology Model with the
571 Penn State–NCAR MM5 Modeling System. Part II: Preliminary Model Validation. *Monthly Weather*
572 *Review*, **129**, 587-604.
- 573 ———, 2001b: Coupling an advanced land surface-hydrology model with the Penn State-NCAR
574 MM5 modeling system. Part I: Model implementation and sensitivity. *Monthly Weather Review*,
575 **129**, 569-585.
- 576 Dudhia, J., 1989: Numerical study of convection observed during the winter monsoon experiment
577 using a mesoscale two-dimensional model. *J. Atmos. Sci.*, **46**, 3077-3107.
- 578 Engelstaedter, S., R. Washington, C. Flamant, D. J. Parker, C. J. T. Allen, and M. C. Todd, 2015: The
579 Saharan heat low and moisture transport pathways in the central Sahara—Multi-aircraft
580 observations and Africa-LAM evaluation. *Journal of Geophysical Research: Atmospheres*, **120**,
581 2015JD023123.
- 582 Garcia-Carreras, L., and Coauthors, 2015: The Turbulent Structure and Diurnal Growth of the
583 Saharan Atmospheric Boundary Layer. *Journal of the Atmospheric Sciences*, **72**, 693-713.
- 584 Han, B., S. Lü, and Y. Ao, 2012: Development of the convective boundary layer capping with a thick
585 neutral layer in Badanjinlin: Observations and simulations. *Adv. Atmos. Sci.*, **29**, 177-192.
- 586 Heinold, B., P. Knippertz, and J. H. Marsham, 2013: Large Eddy Simulations of Nocturnal
587 Low-Level Jets over Desert Regions and Implications for Dust Emission. *EGU General Assembly*
588 *Conference*.
- 589 Heinold, B., P. Knippertz, and R. J. Beare, 2015: Idealized large-eddy simulations of nocturnal
590 low-level jets over subtropical desert regions and implications for dust-generating winds.
591 *Quarterly Journal of the Royal Meteorological Society*, **141**, 1740–1752.
- 592 Heinze, R., D. Mironov, and S. Raasch, 2015: Second-moment budgets in cloud topped boundary
593 layers: A large-eddy simulation study. *Journal of Advances in Modeling Earth Systems*, **7**, 510-536.
- 594 Hong, S.-Y., and H.-L. Pan, 1996: Nonlocal boundary layer vertical diffusion in a medium-range
595 forecast model. *Monthly weather review*, **124**, 2322-2339.
- 596 Hong, S.-Y., and J.-O. J. Lim, 2006: The WRF single-moment 6-class microphysics scheme (WSM6). *J.*
597 *Korean Meteor. Soc*, **42**, 129-151.
- 598 Hu, X.-M., J. W. Nielsen-Gammon, and F. Zhang, 2010: Evaluation of Three Planetary Boundary
599 Layer Schemes in the WRF Model. *Journal of Applied Meteorology and Climatology*, **49**,
600 1831-1844.
- 601 Kain, J. S., 1993: Convective parameterization for mesoscale models: The Kain-Fritsch scheme.
602 *The representation of cumulus convection in numerical models, Meteor. Monogr*, **46**, 165-170.
- 603 Kain, J. S., 2004: The Kain–Fritsch Convective Parameterization: An Update. *JOURNAL OF APPLIED*
604 *METEOROLOGY*, **43**, 170-181.
- 605 LeMone, M. A., M. Tewari, F. Chen, and J. Dudhia, 2013: Objectively Determined Fair-Weather CBL
606 Depths in the ARW-WRF Model and Their Comparison to CASES-97 Observations. *Monthly*
607 *Weather Review*, **141**, 30-54.
- 608 Liu, Y., Q. He, H. Zhang, and A. Mamtimin, 2012: Improving the CoLM in Taklimakan Desert
609 hinterland with accurate key parameters and an appropriate parameterization scheme. *Adv.*
610 *Atmos. Sci.*, **29**, 381-390.
- 611 Liu, Y., and Coauthors, 2011: Simultaneous nested modeling from the synoptic scale to the LES
612 scale for wind energy applications. *Journal of Wind Engineering and Industrial Aerodynamics*, **99**,

- 613 308-319.
- 614 Marsham, J. H., P. Knippertz, N. Dixon, D. J. Parker, and G. M. S. Lister, 2011: The importance of the
615 representation of deep convection for modeled dust - generating winds over West Africa during
616 summer. *Geophysical Research Letters*, **38**.
- 617 Mlawer, E. J., S. J. Taubman, P. D. Brown, M. J. Iacono, and S. A. Clough, 1997: Radiative transfer for
618 inhomogeneous atmospheres: RRTM, a validated correlated-k model for the longwave. *J. Geophys.*
619 *Res.*, **102**, 16663-16682.
- 620 Moeng, C.-H., J. Dudhia, J. Klemp, and P. Sullivan, 2007: Examining Two-Way Grid Nesting for Large
621 Eddy Simulation of the PBL Using the WRF Model. *Monthly Weather Review*, **135**, 2295-2311.
- 622 National Centers for Environmental Prediction, N. W. S. N. U. S. D. o. C., 2015: NCEP GDAS/FNL
623 0.25 Degree Global Tropospheric Analyses and Forecast Grids. Research Data Archive at the
624 National Center for Atmospheric Research, Computational and Information Systems Laboratory.
- 625 Rai, R. K., L. K. Berg, B. Kosović, J. D. Mirocha, M. S. Pekour, and W. J. Shaw, 2017: Comparison of
626 Measured and Numerically Simulated Turbulence Statistics in a Convective Boundary Layer Over
627 Complex Terrain. *Boundary-Layer Meteorology*, **163**, 69-89.
- 628 Schicker, I., D. Arnold Arias, and P. Seibert, 2016: Influences of updated land-use datasets on WRF
629 simulations for two Austrian regions. *Meteorology and Atmospheric Physics*, **128**, 279-301.
- 630 Shin, H. H., and S. Y. Hong, 2011: Intercomparison of Planetary Boundary-Layer Parametrizations
631 in the WRF Model for a Single Day from CASES-99. *Boundary-Layer Meteorology*, **139**, 261-281.
- 632 Shin, H. H., and S.-Y. Hong, 2015: Representation of the Subgrid-Scale Turbulent Transport in
633 Convective Boundary Layers at Gray-Zone Resolutions. *Monthly Weather Review*, **143**, 250-271.
- 634 Skamarock, W. C., and Coauthors, 2008: A Description of the Advanced Research WRF Version 3. .
635 *NCAR/TN-475+STR, NCAR TECHNICAL NOTE*.
- 636 Smirnova Tatiana, G., M. Brown John, G. Benjamin Stanley, and D. Kim, 2000: Parameterization of
637 cold - season processes in the MAPS land - surface scheme. *Journal of Geophysical Research:*
638 *Atmospheres*, **105**, 4077-4086.
- 639 Smirnova, T. G., J. M. Brown, and S. G. Benjamin, 1997: Performance of Different Soil Model
640 Configurations in Simulating Ground Surface Temperature and Surface Fluxes. *Monthly Weather*
641 *Review*, **125**, 1870-1884.
- 642 Stull, R. B., 1988: An Introduction to Boundary Layer Meteorology. *Atmospheric Sciences Library*, **8**,
643 89.
- 644 Sun, J., and Q. Xu, 2009: Parameterization of Sheared Convective Entrainment in the First-Order
645 Jump Model: Evaluation Through Large-Eddy Simulation. *Boundary-Layer Meteorology*, **132**,
646 279-288.
- 647 Talbot, C., E. Bou-Zeid, and J. Smith, 2012: Nested Mesoscale Large-Eddy Simulations with WRF:
648 Performance in Real Test Cases. *Journal of Hydrometeorology*, **13**, 1421-1441.
- 649 ter Maat, H. W., E. J. Moors, R. W. A. Hutjes, A. A. M. Holtslag, and A. J. Dolman, 2012: Exploring the
650 Impact of Land Cover and Topography on Rainfall Maxima in the Netherlands. *Journal of*
651 *Hydrometeorology*, **14**, 524-542.
- 652 WANG, and Coauthors, 2016a: Summer atmospheric boundary layer structure in the hinterland of
653 Taklimakan Desert, China. *Journal of Arid Land*, **8**, 846-860.
- 654 Wang, M., X. Xu, and H. Xu: The possible influence of the summertime deep atmospheric boundary
655 layer process over the Taklimakan Desert on the regional weather. (*submitted to Quarterly Journal*
656 *of the Royal Meteorological Society*).

- 657 Wang, M. Z., H. Lu, H. Ming, and J. Zhang, 2016b: Vertical structure of summer clear-sky
658 atmospheric boundary layer over the hinterland and southern margin of Taklamakan Desert: The
659 deep convective boundary layer of Taklamakan Desert. *Meteorological Applications*, **23**, 438-447.
- 660 Zhang, F., Z. Pu, and C. Wang, 2017: Effects of Boundary Layer Vertical Mixing on the Evolution of
661 Hurricanes over Land. *Monthly Weather Review*, **145**, 2343-2361.
- 662

For Review Only